ERDC/CRREL TR-09-3

Cold Regions Research and Engineering Laboratory

Sea Spray Icing of Drilling and Production Platforms

Kathleen F. Jones and Edgar L Andreas

February 2009

US Army Corps of Engineers®
Engineer Research and Development Center

COVER: Sea spray in the South Atlantic (photo by E. L Andreas).

Sea Spray Icing of Drilling and Production Platforms

Kathleen F. Jones

Cold Regions Research and Engineering Laboratory
U.S. Army Engineer Research and Development Center
72 Lyme Road
Hanover, NH 03755-1290

Edgar L Andreas

NorthWest Research Associates, Inc.
(Seattle Division)
25 Eagle Ridge
Lebanon, NH 03766-1900

Final Report

Approved for public release; distribution is unlimited.

Abstract: Because of the observed decrease in the ice cover in the Beaufort and Chukchi Seas, it is possible that spray icing of rigs used for oil exploration and drilling may be more frequent and possibly more severe in the coming years than it has been in the past. In this report we describe a model for sea spray icing on fixed offshore structures. The accretion of small sea spray droplets onto two-dimensional structural sections and components depends on the liquid water content of the spray cloud, as well as wind speed, droplet diameter, and the diameter of the object. The spray cloud's liquid water content is obtained from the flux of film, jet, and spume droplets from the ocean surface and the vertical velocity of the droplets. The spray droplet flux increases dramatically with increasing wind speed, as whitecaps cover more of the ocean surface and the wind shears droplets off the wave crests. The more massive larger droplets tend to fall out of the spray cloud; as a result, the liquid water content decreases with height. We present modeled icing rates for the semi-submersible drilling rigs *Ocean Bounty* in the winter of 1979-1980 and the *Sedco 708* in January 1983. These results are compared to available information on the icing rate or the ice accumulation.

Contents

Figures and Tables

Figures

Preface

The contents of this report are not to be used for advertising or promotional purposes. Citation of brand names does not constitute an official endorsement or approval of the use of such commercial products.

Unit Conversion Factors

Multiply	By	To Obtain
cubic feet	0.02831685	cubic meters
degrees Fahrenheit	(F-32)/1.8	degrees Celsius
feet	0.3048	meters
knots	0.5144444	meters per second
microns	1.0 E-06	meters
miles (nautical)	1,852	meters
miles (U.S. statute)	1,609.347	meters
miles per hour	0.44704	meters per second
pounds (force)	4.448222	newtons
pounds (force) per foot	14.59390	newtons per meter
square feet	0.09290304	square meters
square miles	2.589998 E+06	square meters

1 Introduction

Because of the observed decrease in the ice cover in the Beaufort and Chukchi Seas, it is possible that spray icing of rigs used for oil exploration and drilling may be more frequent and possibly more severe in the coming years than it has been in the past. While a complete ice cover can result in substantial ice forces on offshore structures, waves are not a problem. In waters with a partial ice cover, wave heights tend to be small, even in high winds. However, the overall decrease in extent of the sea ice cover has left open water in parts of the Beaufort and Chukchi Seas that used to be ice covered. A comparison of the sea ice extent in September 1985 and September 2005 is shown in Figure 1 (http://nsidc.org/data/seaice_index/archives/index.html). Oil exploration platforms and drill rigs operating in these areas now experience more open water and higher waves and, thus, could increasingly suffer from sea spray icing. It would therefore be prudent to provide an icing forecast for these offshore structures operating in open water during subfreezing temperatures, similar to that now provided for vessels by the National Oceanic and Atmospheric Administration (NOAA). This forecast would allow the rig operators to change or curtail operations and to prepare to operate any available de-icing equipment on crucial portions of the structure and gear.
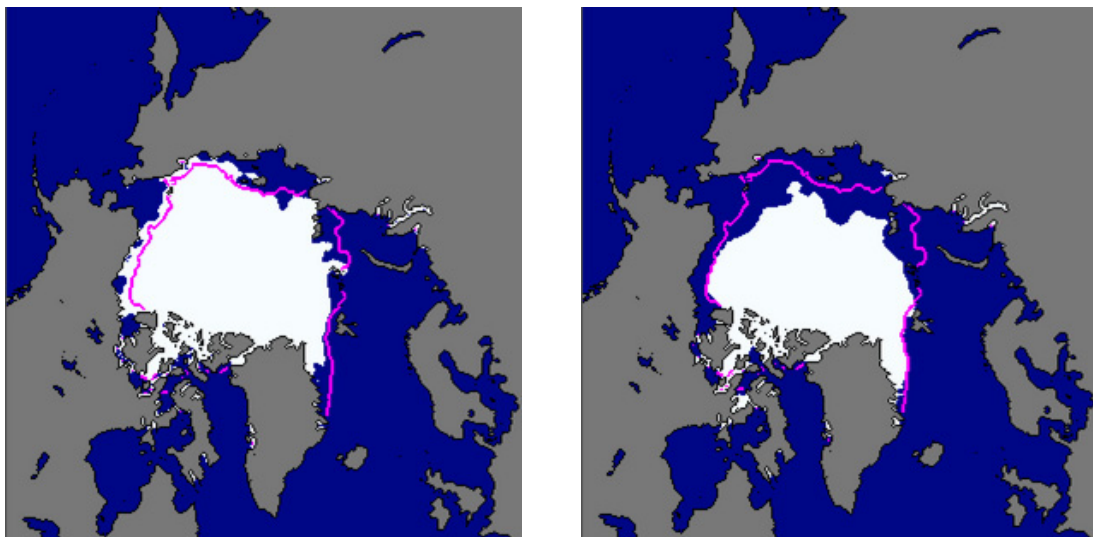
Figure 1. Change in sea ice extent from September 1985 to September 2005. The pink line shows the median ice edge in September.

Platform icing versus ship icing

Sea spray icing of fishing and crabbing boats, coastal freighters, Navy and Coast Guard ships, and tenders for offshore structures in Arctic and northern waters in the winter is a well-known hazard. The weight of ice accreted in the superstructure of relatively small vessels can lead them to lose stability. In these conditions, the vessel often sinks rapidly with the loss of all hands. On larger vessels, in the same conditions, the severity of superstructure icing is less, with the threshold wind speed required to cause spray icing increasing with the length of the ship (Table 5, Overland 1990).

NOAA has produced an ice accretion forecast chart on a daily basis since the winter of 1986-1987 using the Overland et al. (1986) algorithm with a predictor PR that depends on wind speed V, sea temperature T_w, and air temperature T_a:

$$PR = \frac{V\left(T_f - T_a\right)}{1 + 0.4\left(T_w - T_f\right)},$$

(1)

where T_f is the salinity-dependent freezing point of seawater (-1.8°C in the north Pacific). The predictor is related to icing rate (cm h^{-1}) on 20- to 75-m-long trawlers that are headed into or abeam of the wind and not attempting to ameliorate the accretion of ice either by avoiding open seas or by reducing speed. The numerator in Equation 1 represents cooling of the spray water by the air, and the terms in the denominator represent the heat of fusion of the spray that freezes and the cooling of all the spray water to the freezing point. For the ice accretion forecasts, air temperature and wind speed are the 2-m and 10-m values, respectively, from the Global Forecast System model. The sea temperature is obtained from a satellite, ship, and buoy sea-surface temperature analysis. Forecast ice accretions are mapped as light (<0.7 cm h^{-1}), moderate (0.7–2.0 cm h^{-1}), or heavy (>2 cm h^{-1}) on a 10 by 10 grid. A recent example is shown in the National Center for Environmental Prediction 12-hour forecast for 0000 on November 6, 2006, in Figure 2.

Sea spray icing on stationary offshore structures, including oil exploration platforms and drill rigs, is significantly different from sea spray icing on ships. Spray is generated on ships by heaving and pitching as the ship interacts with the waves it is moving through. How individual vessels perform in waves depends on their length, freeboard, stability, and hull

shape; so the icing severity depends on those characteristics of the vessel as well as on the environmental conditions. The majority of the spray that causes ship icing comes from the impact of the water against the hull as the vessel slams into the waves. On the other hand, offshore structures for exploration and drilling, including submersibles, semi-submersibles, and jack-up drilling vessels, are essentially stationary, either sitting directly on the bottom or anchored. They also tend to be relatively open at the water level in contrast to the near-vertical sides of ships. Thus the spray that affects these offshore structures tends to be generated from the waves themselves rather than from the structure-wave interaction.
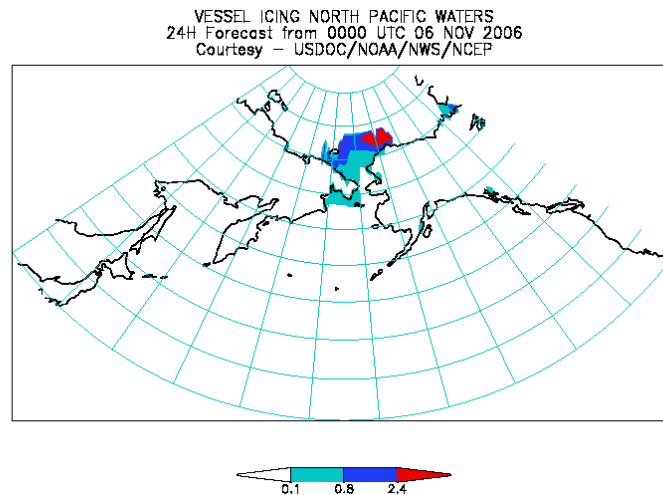
Figure 2. Ice accretion forecast for ships. Units are cm h^{-1}.

The goal of this study is to provide algorithms for processing weather data to determine sea spray icing severity on offshore structures. Input to the algorithms is data from offshore platforms, buoys, or stations on the coast with hourly measurements of wind speed and air temperature. For coastal stations, only data from periods with onshore winds should be used so that over-ocean conditions are represented. Ultimately, these algorithms could be used with forecast wind speeds and temperatures to forecast icing severity on drill rigs, similar to the vessel icing forecasts that are currently available (Figure 2). With such a forecast, the operators of drill rig and oil exploration platforms could prepare to deploy anti-icing and deicing measures and curtail operations to an extent determined by the severity of the expected icing conditions. Icing is a safety issue for workers on the vessels and can also immobilize exposed mechanical devices and thereby limit both communications and operations.

Organization

In Section 2 we review the formulation for the accretion of small droplets on two-dimensional structural sections (e.g., cables, guys, angles, channels, W-sections) and components (e.g., handrails, ladders, antennas, winches). Particular attention is paid to the collision efficiency of the spray droplets and the effects of wind speed, droplet diameter, and the diameter of the component. The use of the median volume diameter to characterize the spray droplet cloud is discussed. In Section 3 we introduce the formulation for the flux of spray droplets from the ocean surface. The physical mechanisms of spray droplet formation are briefly described and references with more detailed discussions are provided. The empirical relationships between significant wave height and wind speed as well as whitecap generation and wind speed are presented and their limitations are discussed. The calculation of the spray droplet concentration distribution at the sea surface from the spray flux is discussed and the expected vertical variation in the spray droplet profile is derived. The calculated concentration distributions at half the significant wave height are compared to measured values from the literature. In Section 4 we present model results for sea spray icing on the *Ocean Bounty* semi-submersible exploratory drilling rig in the winter of 1979-1980 and the *Sedco 708* semi-submersible drilling rig in January 1983. These results are compared to available information on the icing rate or the ice accumulation. Limitations of the current state of knowledge and suggestions for further studies are discussed in Section 5.

2 Ice Accretion

Sea spray icing on fixed offshore platforms occurs when wind-blown water droplets generated from whitecaps on the ocean surface strike a portion of the platform structure and freeze (Figure 3). We expect icing to be more severe at lower heights above the ocean surface, both because the droplets tend to evaporate as they are transported from their source and because larger droplets tend to fall out of the spray cloud because of gravity. On the other hand, no ice is expected to accrete near the waterline, where the structure is warmed by the water as waves and swell wash over it. Because the spray droplets are carried by the wind, more ice is expected to accrete on the windward side of the platform and on the windward side of structures and components on the platform. Ice will also accumulate on top of horizontal surfaces as water flows off vertical surfaces or drips off cables, handrails, and other elevated components when it is not cold and windy enough to freeze the impacting droplets immediately.

Figure 3. Sea spray icing on the *Ocean Bounty* in the winter of 1979-1980 in Lower Cook Inlet (photo provided by MMS).

The spray cloud is characterized by its liquid water content distribution (units are $g\,m^{-3}\,\mu m^{-1}$):

$$w(z,r) = \frac{4}{3}\pi r^3 \rho_w c(z,r)$$, (1)

where ρ_w is the density of sea water (kg m^{-3}), z is height above the ocean surface (m), and r is the droplet radius (μm). The concentration distribution of the spray droplets $c(z,r)$ is the number of droplets per cubic meter of air per micron increment in radius (m^{-3} μm^{-1}). The important meteorological parameters are wind speed and air temperature. The most severe icing will occur in events with high winds and subfreezing temperatures for extended periods.

The icing rate on a cylinder is

$$\frac{dT(z)}{dt} = \frac{U(z)D}{\rho_i} \int_{r_{min}}^{r_{max}} E(U,r,D)w(z,r)dr ,$$ (2)

where:

$T(z)$ = ice thickness (mm)
t = time (s)
$U(z)$ = wind speed (m s^{-1})
D = cylinder diameter (m)
ρ_i = ice density (kg m^{-3})
$E(U, r, D)$ = collision efficiency of the droplets with the cylinder.

The collision efficiency is a number between 0 and 1 that is the portion of the mass of droplets that are swept out by the cylinder that actually hit the cylinder. It results from a balance between inertia, which tends to keep the droplets traveling in a straight line, and drag, which tends to make the droplets follow the wind streamlines around the cylinder. Collision efficiencies for cylinders were computed on an analog computer and provided in tabular graphical form in Langmuir and Blodgett (1946) and recomputed with better drag formulations on a digital computer and provided as convenient formulas by Finstad et al. (1988a).

A simplification of Equation 2 is obtained by using the median volume radius r_M, which is the radius for which half the liquid water content $W(z)$ is in larger droplets and half is in smaller droplets:

$$\frac{W(z)}{2} = \int_{r_{\min}}^{r_M} w(z,r)\,dr.$$
(3)

It has been shown for cloud droplet distributions (Finstad et al. 1988b) that

$$\int_{r_{\min}}^{r_{max}} E(U,r,D)w(z,r)\,dr \approx E(U,r_M,D)W(z),$$
(4)

so that Equation 2 simplifies to

$$\frac{dT(z)}{dt} = \frac{U(z)DE(U,r_M,D)W(z)}{\rho_i}.$$
(5)

The range of drop radii from sea spray (nominally 0.1–500 μm) is much larger than the typical range in clouds (1–50 μm), so in practice Equations 4 and 5 are applied over segments of the spray droplet distribution. The liquid water content distribution, characterized by the distribution at n specific radii r_j, is integrated numerically to obtain the liquid water content using the trapezoid rule. The median volume radius r_{Mj} for that portion of the distribution is

$$r_{Mj} = r_{j-1} + \left[-\frac{w_{j-1}}{w_j - w_{j-1}} \pm \sqrt{\left(\frac{w_{j-1}}{w_j - w_{j-1}}\right)^2 + \frac{1}{2}\frac{(w_j + w_{j-1})}{w_j - w_{j-1}}} \right](r_j - r_{j-1}),$$
(6)

where we use the plus sign when $w_j > w_{j-1}$ and the minus sign when $w_j < w_{j-1}$. The collision efficiency is then determined for each r_{Mj}, and the icing rate in Equation 5 is a summation over the n droplet radii:

$$\frac{dT(z)}{dt} = \frac{U(z)D\sum_{j=1}^{n} E(U,r_{Mj},D)W_j(z)}{\rho_i}.$$
(7)

The icing rate on representative structural components is straightforward to compute given the concentration distribution of droplets in the spray cloud. Because the droplets cool rapidly from the sea temperature to a temperature lower than the air temperature, a heat balance calculation,

such as was done for freezing rain in Jones (1996), is not necessary. This dry accretion (i.e., flux limited) assumption (Jones 1998) may be slightly conservative at air temperatures near freezing, causing us to overestimate the amount of ice that accretes. However, its simplicity more than compensates for these occasional overestimates.

At typical ocean salinities, the freezing point is -1.8°C. The droplets will tend to reject brine as they freeze, leaving a salty liquid surface layer on the frozen droplet. Except in relatively warm conditions with high liquid water contents, the droplets freeze individually incorporating small air inclusions. Thus the ice accumulates as an ice-water-air matrix with a density that depends on the weather conditions and the location on the platform. Ryerson and Gow (2000) measured the density of ice accreted on the superstructure of the Coast Guard cutter *Midgett* in the Bering Sea in 1990. The density of 17 samples taken from various locations ranged from 690 to 920 kg m^{-3}, with a median of 850 kg m^{-3}. They also summarize density data from other authors, reporting an overall range from 620 to 940 kg m^{-3}. For this study we do not attempt to model the ice density but assume a relatively high density of 900 kg m^{-3}. At cold temperatures and relatively low spray concentrations, densities are likely to be lower than this. In these conditions, which can occur with moderate whitecap coverage at low heights on the drill rig or with significant whitecap coverage higher on the rig, the thickness of lower density ice will be greater than the modeled thickness. However, the modeled thickness with the assumed density correctly represents the accreted mass of ice.

The icing rate profile in Equation 7 is calculated throughout the spray icing event using the time-varying measured wind speed and air temperature and modeled droplet concentration density. To estimate the wind speed profile, we use the standard formulation for the atmospheric surface layer, which is based on the air-sea temperature difference and the measured wind speed at one height (e.g., Andreas 1998). Andreas et al. (2008) describe the specific algorithm that we use. The spray generation function, from which the droplet concentration is obtained, increases as the third power of wind speed. The collision efficiency E also increases with wind speed. Thus the rate of ice accretion in Equation 7 increases with at least the fourth power of wind speed, and the icing rate for a wind speed of 20 m s^{-1} is more than 16 times the icing rate for a wind speed of 10 m s^{-1}.

3   Spray

Sea spray fluxes

An icing forecast for fixed structures is based on the potential for sea spray generation by the wind. Sea spray droplets are produced by three mechanisms (Andreas 2002). Wind creates breaking waves; these waves trap air that manifests as whitecaps on the surface. These whitecaps are clouds of bubbles; when the bubbles rise to the surface and burst, they fling into the air small "film" droplets and larger "jet" droplets (Monahan 1986; Monahan et al. 1986). The small film droplets, ranging from 0.5 to 50 μm in radius are produced as air bubbles in a whitecap burst and the bubble film shatters into water droplets. Jet droplets, ranging from 1 to 100 μm in radius, are produced as the collapsing whitecap bubble shoots up a jet of water that breaks into droplets. Spume droplets, also called spindrift, are formed by the wind's shearing droplets off the wave crests; these range in radius from 20 to 500 μm. The peak in the volume flux of droplets—that is, the range that carries most of the airborne water—occurs in the spume size range. At about 10 m s^{-1}, the winds are strong enough to create whitecaps covering 1% of the sea surface and tear droplets off the wave crests. With winds of 20 m s^{-1}, whitecaps cover 10% of the sea surface. Because spray generation follows whitecap coverage, it increases at roughly the third power of wind speed (Monahan et al. 1986).

The key piece of information for this study is the rate at which spray droplets are produced. This spray generation function is denoted dF/dr, and has units of number of droplets produced per square meter of sea surface area, per second, per micron increment in droplet radius (m^{-2} s^{-1} μm^{-1}). In the field of marine aerosol science there has been quite a bit of controversy as to the magnitude and form of the spray generation function. Significant advances in understanding and quantifying sea spray generation occurred as a result of the HEXOS (Humidity Exchange Over the Sea) program that began in the early 1980s. Andreas (2002) reviewed about a dozen published sea wave spray generation functions. He used known relationships among the different droplet sizing conventions to convert each of the published spray generation functions into terms of the spray droplet radius at creation at the level of the sea surface r_0. Some of the functions had to be adjusted from measurement heights of tens to hundreds of meters above the sea surface. He made these adjustments using a formulation provided

by Fairall and Larsen (1984) for the vertical transport of droplets. Andreas discarded most of the published functions because they violated theoretical constraints on the magnitude of the function and its wind speed dependence and concluded that the spray generation function that Fairall et al. (1994) developed had the best properties.

The Fairall et al. function estimates the rate of formation of spray droplets with r_0 between 1.6 and 500 μm. For this study we extended it to even smaller droplets using the "bubbles-only" function reported by Monahan et al. (1986). It treats film droplets as small as 0.5 μm and has proven useful in many other studies of marine aerosols (e.g., Burk 1984; Stramska 1987; Gong et al. 1997). Moreover, because it has the same wind speed dependence as the Fairall et al. (1994) function, it was easy to create a spray generation function that treats droplets with r_0 from 0.5 to 500 μm by simply matching the Monahan et al. and Fairall et al. functions at r_0 = 2.0 μm.

Because we are ultimately interested in the mass flux of the spray, we usually present the spray generation function as a volume flux $\left(4\pi r_0^3 / 3\right) dF / dr_0$. The merged spray generation volume flux is plotted in Figure 4 for droplet radii r_0 between 0.5 and 500 μm for four wind speeds. The equilibrium radius for droplets in air of 80% relative humidity r_{80} is roughly half of r_0; $r_{80} \approx 0.5 r_0$. The figure shows that the rate at which spray is generated increases dramatically with wind speed. The figure also suggests that droplets with radii of 100 to 200 μm carry most of the mass away from the sea surface. These droplets are almost all spume droplets—those ripped right off the wave crests by the wind.

The concentration distribution of the droplets $c(z,r)$ in the air depends on the height above the water surface z and the droplet radius r and can be determined from the concentration at the ocean surface. Spray droplets start with initial radius r_0 and with the same temperature as the surface ocean water T_w but begin evolving in both temperature and size once they are ejected into the air. Figure 5 shows the evolution of a droplet with 100-μm initial radius created in water that is at the freezing point -1.8°C and then ejected into air with a much lower temperature, say, -10°C. These results are from the microphysical spray model that Andreas (1989) developed from ideas and equations in Pruppacher and Klett (1978).

Figure 5 makes several essential points. First, this 100-μm droplet cools from the water temperature to a temperature below the ambient air temperature in about 2 s. The smaller droplets cool to temperatures below the ambient air temperature in even less time. In typical Arctic conditions, the spray droplets are thus supercooled and will freeze quickly if they hit a structure with a surface temperature that is below freezing.

The second point that Figure 5 makes is that, though the droplets cool very rapidly, they evaporate much more slowly—the evaporation rate is about three orders of magnitude slower than the cooling rate regardless of droplet size. Furthermore, because the droplets are saline, they do not evaporate entirely but, rather, reach an equilibrium radius that is no smaller than half the original radius for typical humidities and Arctic Ocean salinities. For example, the 100-μm droplet in Figure 5 retains nearly its original radius for almost 100 s, and takes 2000 s to evaporate to a 60-μm-radius droplet. For this study we assume that the droplets not only cool to the air temperature but also evaporate to their equilibrium size at 80% humidity before being blown onto the superstructure of an offshore platform.
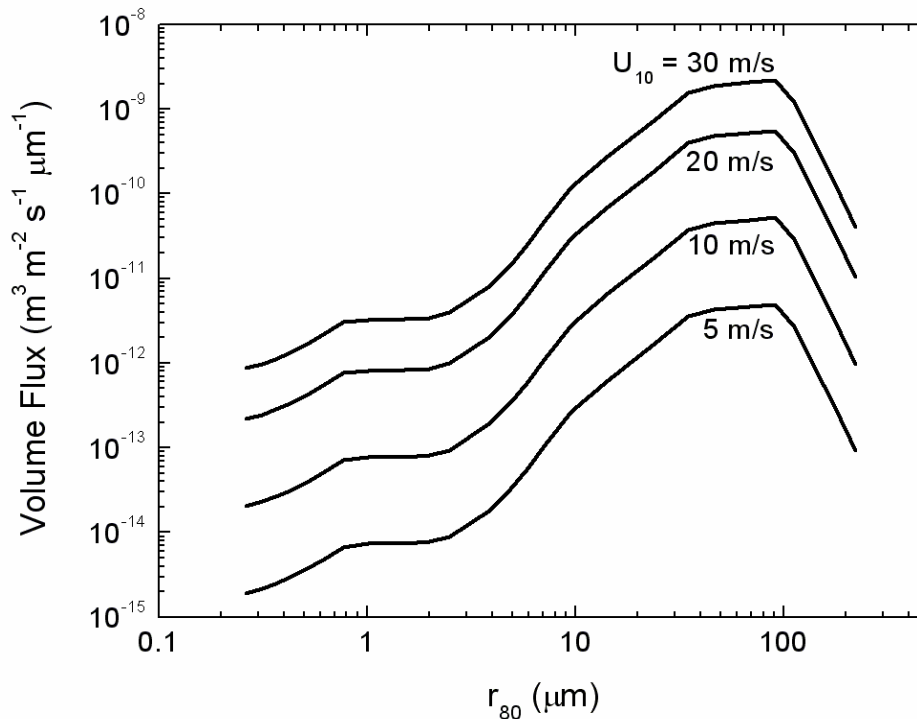
Figure 4. The spray generation function for this study is expressed in terms of a volume flux $\left(4\pi r_{80}^3 / 3\right) dF / dr_{80}$, where r_{80} is the droplet radius in equilibrium at a reference relative humidity of 80%. This function is a synthesis of functions reported by Monahan et al. (1986) and Fairall et al. (1994). U_{10} is the wind speed at a height of 10 m.
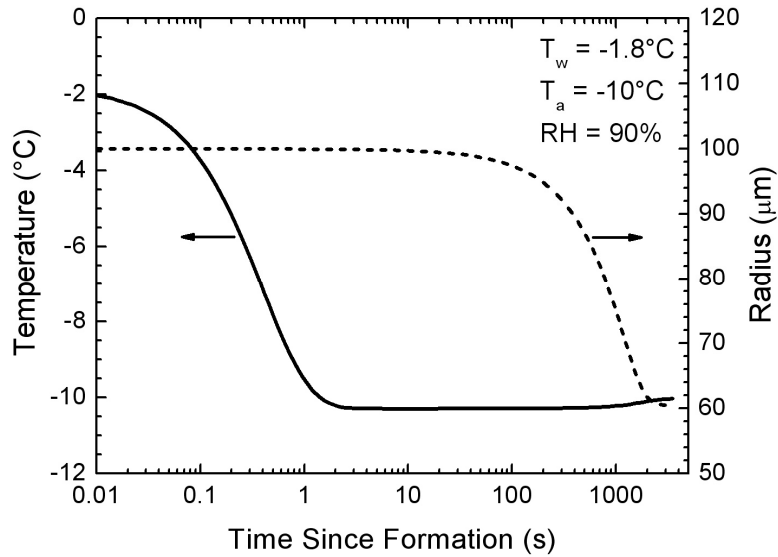
Figure 5. The evolution in temperature and radius of a droplet with 100-μm initial radius that formed from water with temperature -1.8°C and is ejected into air with temperature -10°C and relative humidity 90%. The barometric pressure is assumed to be 1000 mb, and the surface salinity is 34 psu.

Significant wave height

The significant wave height $H_{1/3}$ is the average height of the highest one-third of the waves. The height of wind waves increases with the square of the wind speed and also depends on the water depth D_w. Andreas and Wang (2007) determined a relationship between U_{10} (m s^{-1}) and $H_{1/3}$ (m) based on buoy data in the North Atlantic off the east coast of the United States:

$$H_{1/3} = c(D_w) \text{ for } U_{10} \le 4 \text{ m s}^{-1}$$
$$H_{1/3} = a(D_w)U_{10}{}^2 + b(D_w) \text{ for } U_{10} > 4 \text{ m s}^{-1}$$
with
$$c(D_w) = 1.36 \tanh\left[\frac{\ln(D_w/6)}{1.9}\right] \tag{8}$$
$$a(D_w) = 0.0134 \tanh\left[\frac{\ln(D_w/9)}{1.3}\right]$$
$$b(D_w) = c(D_w) - 16a(D_w).$$

The measured significant wave heights are scattered about the values calculated from Equation 8 because of variations in fetch, swell, the stability

of the atmosphere, and the duration of the wind. It is not known how well this parameterization represents conditions off the Alaskan coast.

Whitecap coverage

The availability of spray droplets is determined by the whitecap cover on the surface of the ocean. For wind speeds below about 3 m s^{-1} there are no whitecaps. The fraction of the ocean surface that is covered by whitecaps f_{wc} is estimated from the wind speed at 10 m using a relation from Monahan and Muircheartaigh (1980)

$$f_{wc} = 3.84x10^{-6}U_{10}{}^{3.41}. \tag{9}$$

Note that 100% whitecap cover is obtained for U_{10}=39 m s^{-1}. The data underlying Equation 9 is for relatively warm water (20°C < T_w < 30°C), and U_{10} < 20 m s^{-1}. Those authors suggest that the water temperature affects the mean lifetimes of whitecaps, and the air-water temperature difference also influences whitecap coverage.

Monahan et al. (1983) suggest that whitecap cover depends on wind duration and fetch as well as on speed and, in shallow water, depends on the bathymetry of the ocean floor. In viscous cold water, whitecap coverage will be less than in less viscous warm water under the same meteorological conditions because the ocean is more efficient in dissipating the energy input by the wind; hence, fewer breaking waves are created. Wu (1988) suggests that f_{wc} is related to the cube of the friction velocity u_*, which is proportional to the rate of energy supplied by the wind per unit area of the ocean surface. Using the friction velocity rather than the wind speed implicitly incorporates atmospheric stability in the determination of f_{wc}. Piazzola et al. (2002) use physical relationships to incorporate fetch limitations in their whitecap cover equation.

Spray concentration profile

de Leeuw et al. (in preparation) develop a new theoretical model for the relationship between dF/dr and the droplet concentration distribution $c(z,r)$ as a function of height z and droplet radius r. This model builds on earlier work by Fairall and Larsen (1984) and Hoppel et al. (2002, 2005) and uses concepts that treat particle deposition, as originally formulated by Slinn et al. (1978) and Slinn and Slinn (1980). We sketch just the rudiments of that model here.

Conceptually, we assume that all spray droplets are formed at some reference height h above mean sea level. Because spray generation is closely associated with breaking waves and the mechanical tearing of wave crests, a good choice for h is $0.5H_{1/3}$, half the significant wave height. We assume that for $0 \leq z \leq h$

$$F_T - \frac{dF}{dr} = -V_{dh}c_h,$$

(10)

where F_T is the net turbulent flux of spray droplets. Specifically,

$$F_T = \overline{w'c'(r)}$$

(11)

is a typical vertical Reynolds flux, where w' is the turbulent fluctuation in vertical velocity and $c'(r)$ is the turbulent fluctuation in the concentration distribution of droplets with radius r. The overbar denotes a time average that typically is 30–60 minutes. As with most Reynolds fluxes in the near-surface atmosphere, F_T is assumed to be constant with height. For simplicity $c(h,r)$, the spray concentration distribution at height h, is written as c_h. Also in Equation 10,

$$V_{dh} = \frac{V_g + V_a}{1 + \dfrac{V_a}{V_g}\left(1 - f_{h\delta}\right)}$$

(12)

is the deposition velocity for droplets of radius r at height h. V_g is the terminal fall speed of droplets with radius r, always assumed positive, V_a is a diffusive velocity described in Appendix A, and

$$f_{h\delta} = \left(h/\delta\right)^{-V_g/ku_*}.$$

(13)

Here $k = 0.40$ is the von Kármán constant; u_* is the friction velocity, a dynamic velocity scale of the atmospheric surface layer; and

$$\delta = \frac{\Lambda\nu}{u_*}$$

(14)

is the approximate thickness of the molecular diffusion layer at the ocean surface, where ν is the kinematic viscosity of air and Λ is a constant that we take as 5 (de Leeuw et al. in preparation).

For droplets above the source, $dF/dr = 0$, and the governing equation is

$$F_T = -V_g \left(\frac{c_z - f_{zh} c_h}{1 - f_{zh}} \right),$$ (15)

where c_z is $c(z,r)$ and

$$f_{zh} = (z/h)^{-V_g/ku_*}.$$ (16)

On substituting Equations 12 and 15 in Equation 10, we obtain

$$\frac{\left[1 + \dfrac{V_a}{V_g}(1 - f_{z\delta})\right] c_h}{1 + \dfrac{V_a}{V_g}(1 - f_{h\delta})} - \frac{(1 - f_{zh})dF/dr}{V_g} = c_z,$$ (17)

where

$$f_{z\delta} = (z/\delta)^{-V_g/ku_*}.$$ (18)

Notice that Equation 17 relates the spray concentration distribution c_z to the spray generation function dF/dr if we know c_h, the concentration at height h.

Spray concentration distribution at the surface

We test three assumptions for estimating the surface concentration distribution c_h for use in Equation 17 from the known dF/dr. Hoppel et al. (2005) and de Leeuw et al. (in preparation) suggest that the upward flux of droplets must be the same as the downward flux, which means that the deposition velocity of the droplets should be used to determine the concentration from the flux:

$$\frac{dF}{dr} = V_{dh} c_h.$$ (19)

According to Equation 10, this assumption implies $F_T = 0$.

A second estimate of c_h comes from using the droplet ejection velocity V_{ej} as suggested by Monahan (1968). This is the initial upward velocity of the jet droplets that are created by collapsing bubbles. Blanchard (1963) obtained the ejection velocity for droplets with radii between 1.5 and 335 μm from laboratory measurements. This ejection velocity takes the place of V_{dh} in Equation 10:

$$\frac{dF}{dr} = V_{ej}c_h.$$ (20)

A third method for estimating c_h is based on postulating that the friction velocity u_* is the appropriate scale to obtain c_h from dF/dr. Spray droplets are freed from the sea surface by bursting bubbles or by some other instability mechanism. Once free, they naturally tend to fall back into the sea. Only if turbulence in the air suspends them do they have any appreciable residence time. In models, such turbulent suspension and dispersion is parameterized in terms of the Langevin equation (e.g., Edson and Fairall 1994; Pattison and Belcher 1999) in which the rate that droplets move up and down in response to the turbulence is related to σ_w, the standard deviation of the wind's vertical velocity component. Because $\sigma_w \approx 1.25u_*$, u_* is a reasonable scale for relating c_h and dF/dr. Thus,

$$\frac{dF}{dr} = u_*c_h.$$ (21)

In all three cases, c_z is obtained from c_h using Equation 17 and the result that $F_T = 0$.

Deposition, ejection, and friction velocities are compared in Figure 6. The ejection and deposition velocities differ by more than 3 orders of magnitude for small droplets but are nearly the same for droplet radii of a few hundred microns. Friction velocities tend to be between the ejection and deposition velocities, varying with wind speed and atmospheric stability rather than with droplet size.

The effects of these three assumptions for determining c_h from dF/dr are significant. Note that for a given flux, higher droplet velocities imply smaller droplet concentrations. Calculated spray liquid water content pro-

files are shown in Figure 7a for U_{10} = 20 m s^{-1}. Liquid water contents based on the deposition velocity assumption are much higher than those obtained from using either the ejection velocity, which results in extremely small liquid water contents, or friction velocity. Figure 7b shows the cumulative contribution to the liquid water content at 5 and 50 m above sea level (asl) over the range of droplet sizes. Because of the extremely small deposition velocities of small droplets, they contribute significantly to the liquid water content at 5 m, and even more so at 50 m, where the larger droplets are less numerous. On the other hand, large droplets have a significant contribution to the liquid water content based on ejection velocity because of their relatively low initial velocity.
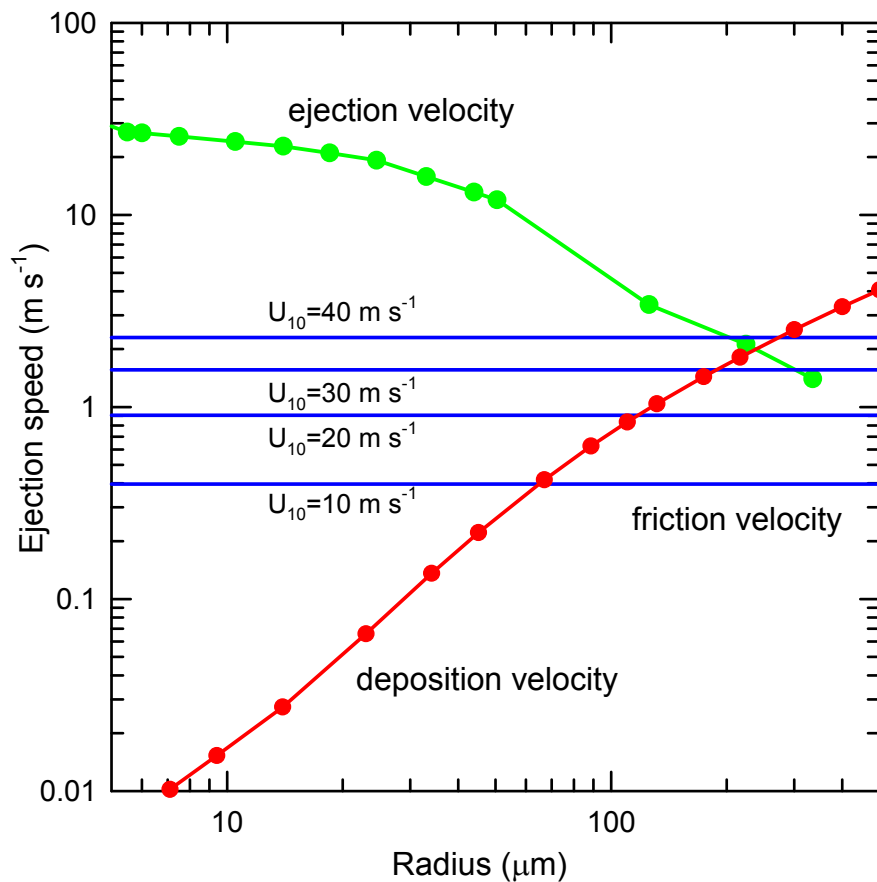
Figure 6. Variation of deposition and jet droplet ejection velocities with spray droplet radius; variation of friction velocity with U_{10}.

We can compare our calculated c_h values to measured values. Concentration distribution profiles have been published by Monahan (1968) and de Leeuw (1986a,b, 1987). Measured c_h values for wind speeds of 12.4 m s^{-1} in the North Sea (de Leeuw 1987), 13 m s^{-1} (de Leeuw 1986a) in the North At-

lantic, 11 m s⁻¹ near Aruba, and 16 m s⁻¹ in Buzzards Bay (Monahan 1968) are compared to calculated values for a wind speed of 13 m s⁻¹ at 25 m asl with a 2.5-m significant wave height in Figure 8. In these comparisons, all droplet characteristics are evaluated in terms of r_{80}, the droplet radius at equilibrium for a relative humidity of 80%. That is, in Equation 19, for example, $dF/dr = dF/dr_{80}$. All the calculated c_h values agree well for droplets with radius greater than about 100 μm, but in this range they are smaller than Monahan's measured values. For droplet radii less than 20 μm, the
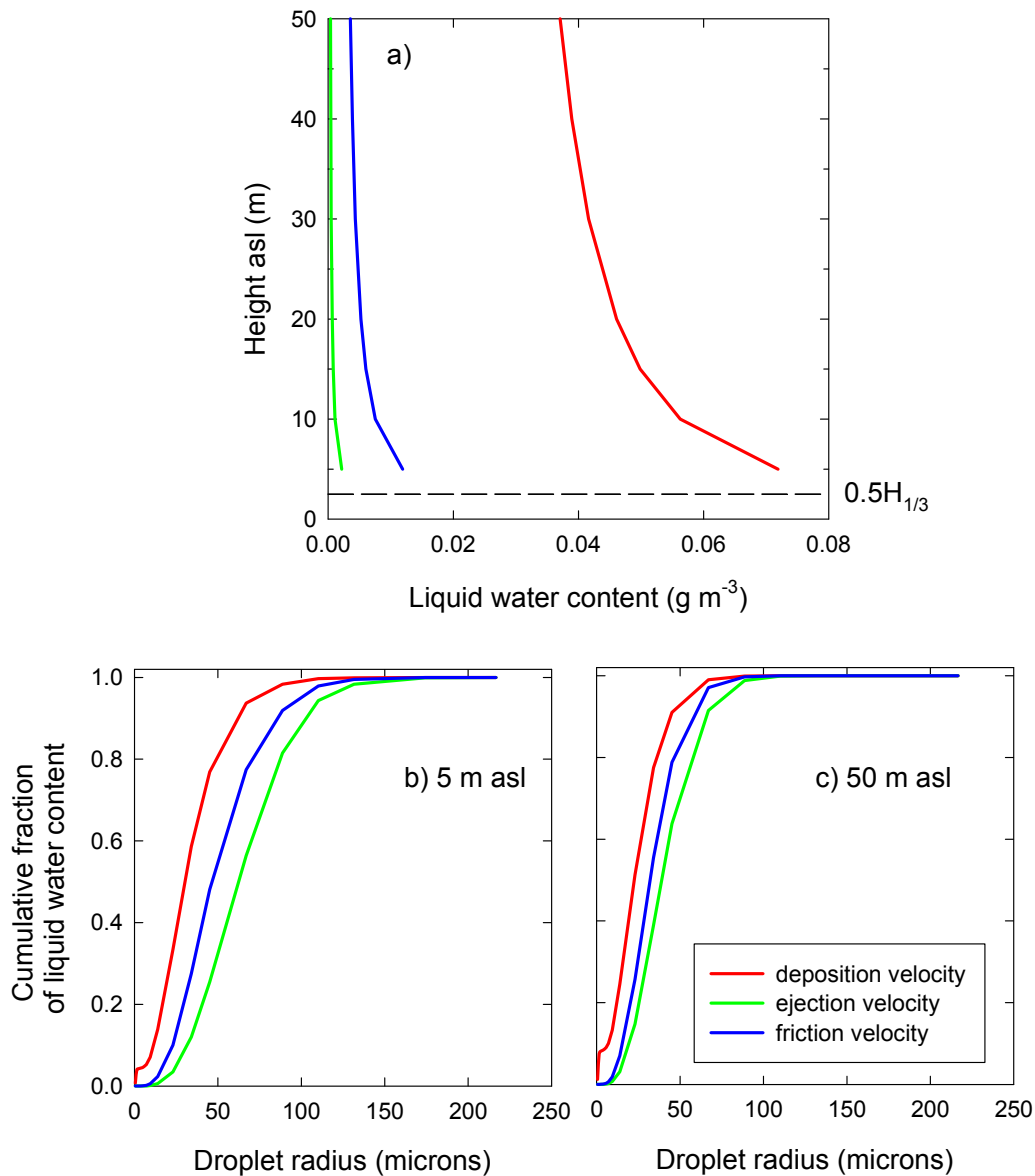
Figure 7. Results of concentration calculation at the ocean surface for U_{10} = 20 ms⁻¹; comparison of deposition, ejection, and friction velocity assumptions: (a) liquid water content profile; contribution of droplets to the liquid water content, over the range of droplet radii, at (b) 5 m asl and (c) 50 m asl.

ejection velocity c_h is too small by up to an order of magnitude compared to de Leeuw's measured values. The deposition velocity c_h has roughly the same shape as de Leeuw's data for small droplets but is too large by one or two orders of magnitude. The friction velocity c_h has the same magnitude as the de Leeuw values for small droplets, but the curve is very flat in comparison, implying that droplets with radii less than about 20 μm are equally numerous.

We further test these three concentration assumptions in Section 4 by using them to determine the spray cloud liquid water content distribution during icing events for two drill rigs in Alaskan waters. We can then compare those rates to the observed icing severity.
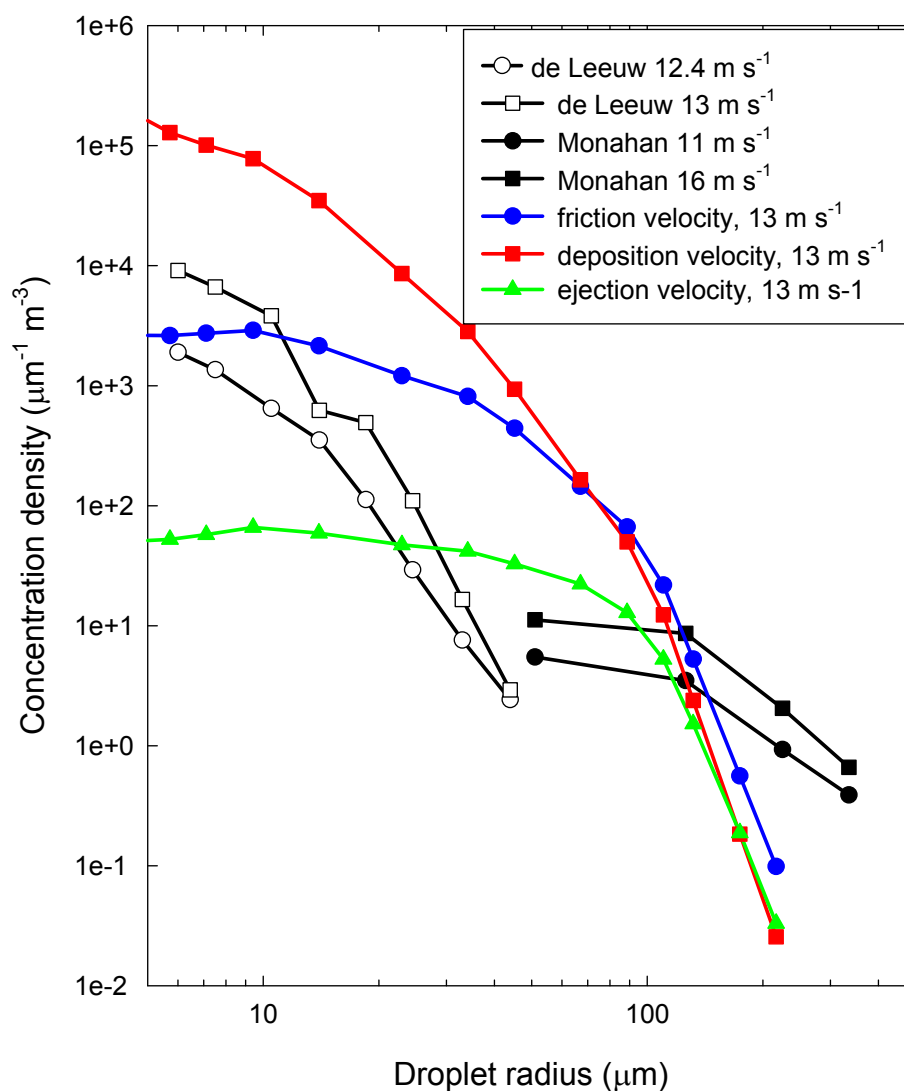
Figure 8. Measured sea spray concentration densities at the ocean surface compared to calculated values based on the three droplet velocity assumptions.

4   Icing Cases

Data are available from only two semi-submersible drilling rigs in sea spray icing events. Severe sea spray icing affected the *Ocean Bounty* and the nearby *Dan Prince* during the winter of 1979-1980 in Cook Inlet, Alaska. Six distinct events occurred during the 121-day period that the *Ocean Bounty* was on station. So much ice accumulated on the superstructure in one event that drilling mud had to be offloaded to keep the vessel from losing buoyancy. These severe events instigated icing studies by Minerals Management Service, including one led by Cold Regions Research and Engineering Laboratory's David Minsk (now retired) on the semi-submersible vessel *Sedco 708* on the North Aleutian Shelf during the fall and winter of 1982-1983. These two data sets are presented and discussed here, with model estimates of the spray icing intensity.

Sedco 708

The semi-submersible drilling rig *Sedco 708* (Atlantic Venture) was deployed by ARCO Alaska for the Continental Offshore Stratigraphic Test at 56.274°N, 161.976°W in 53 m of water (Figure 9). The *Sedco 708* main deck was about 128 ft above the bottom of the pontoons. The normal drill-
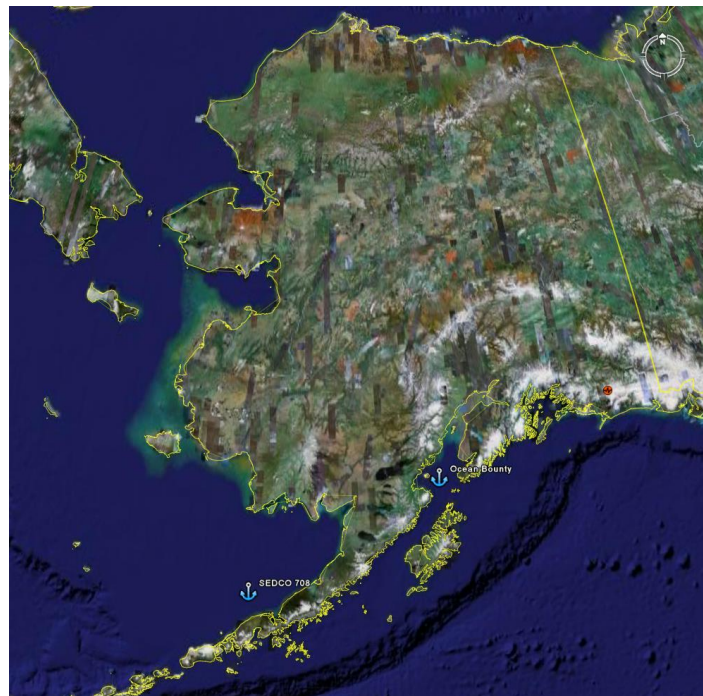
Figure 9. Location of *Ocean Bounty* and *Sedco 708*.

ing draft of 85 ft puts the main deck at about 43 ft (13 m) above the ocean surface. An ice accretion observation program and the evaluation of candidate ice-phobic coatings were included as part of the drilling program. The information provided here on the observation program is from Minsk (1984a, 1985). Three Rosemount model 872DC ice detectors were mounted on the 180-ft-tall derrick, with a fourth at about 20 ft above deck on the railing on the roof of the diving bell storage area. In addition, six arrays of 8-in.-long, $1^{15}/_{16}$-in.-diameter cylinders were mounted just below the main deck in accessible locations, with reasonable exposure to sea spray icing. Five panels with candidate ice-phobic coatings applied to 1-ft-square steel plates were also mounted below the main deck.

Only two significant storms occurred while the drilling rig was on station: one in early December 1982 that was not documented, and one from January 3 through January 8, 1983. Hourly weather and sea conditions during that storm are shown in Figure 10. Wind speeds reached as high as 20 m/s with gusts over 25 m/s, concurrent with air temperatures as cold as -10°C. Measured significant wave heights (bottom panel) were almost six meters with good agreement between the measured and modeled values from Equation 8. The water temperature decreased from 3.9°C to 3.3°C during this period.

No icing was measured by the Rosemount ice detectors on the derrick or the railing. Up to about 5 in. of ice accumulated on the diagonal cylindrical trusses in the middle of the below-decks structure, but, surprisingly, there was no ice accumulation at the same level on the windward side of the platform. The lower third of the trusses was kept clear by waves; above that level the ice thickness decreased with height as the bottom of the deck was approached. Up to about 1 in. of ice accumulated on the cylinder arrays. That is only a rough estimate because the arrays were inaccessible during the storm. A total of about 30 tons of ice accumulation was estimated, based on the observed distribution of ice thicknesses and the amount of ballast that had to be pumped to maintain trim.

To model the accretion of spray ice during this storm, a number of assumptions had to be made. Assuming the anemometer is mounted at 20 m above the sea surface results in the calculated 10-m wind speed shown in the middle panel of Figure 10. An unstable atmosphere is assumed, with the air heated from below by the warmer water. Thus the vertical mixing of the spray droplets is greater than it would be in stable conditions, leading

to relatively small vertical droplet concentration gradients. The vertical variation in the liquid water content is calculated based on the droplet concentration distribution calculated from the droplet concentration at $z = 0.5H_{1/3}$. That in turn is determined from the spray droplet flux at the ocean surface divided by either the droplet deposition velocity, the droplet ejection velocity, or the friction velocity, as discussed in Section 4. The icing rate for each hour is determined for cylinder diameters ranging from 0.5 to 30 cm, incorporating the effect of collision efficiency. These icing rates are based on the assumption that the ice freezes instantaneously on the windward side of the cylinder, with the ice-covered cylinder retaining
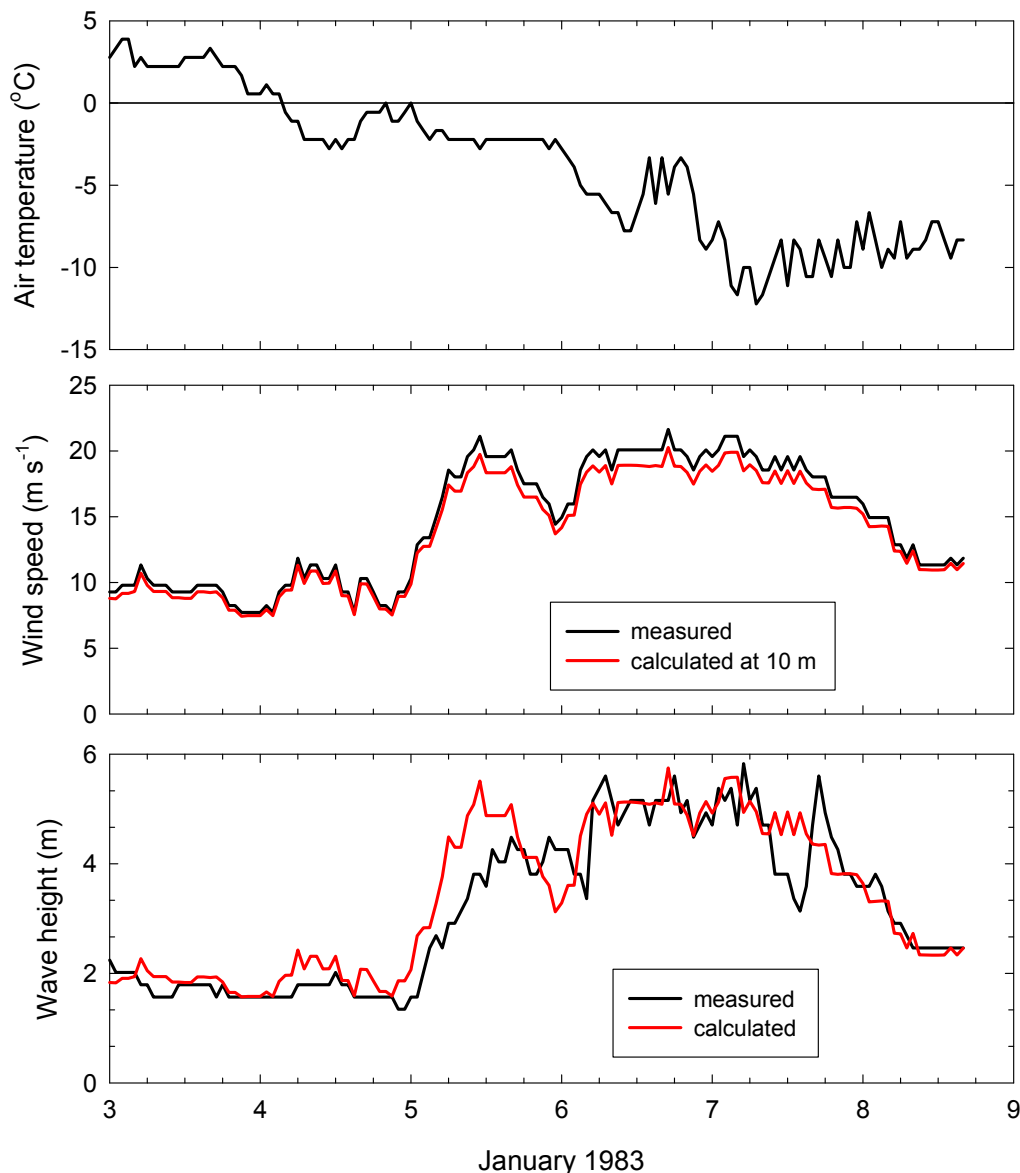
Figure 10. Measured air temperature, measured wind speed and calculated 10-m wind speed, and measured and calculated significant wave height for *Sedco 708*.

the same projected area perpendicular to the wind direction throughout the storm. The accumulation of ice at approximately the level where ice was observed on the large cylindrical diagonal trusses is shown in Figure 11a for all three droplet velocity assumptions. The accumulation of ice at the level of the cylinder arrays and just above the main deck level is shown in Figure 11b. These results can be compared to the 5 in. and 1 in. of ice that was estimated on the trusses and the cylinders, respectively. Keep in mind that the 25-mm increments on the vertical axes in Figure 11 are about 1 in.

Ocean Bounty

Spray icing of the semi-submersible exploratory drilling rig *Ocean Bounty* operated by Phillips Petroleum Company during the winter of 1979-1980 is described in Williams (1981), Nauman (1984), Nauman and Tyagi (1985), and Minsk (1984b). The *Ocean Bounty* was on station near Kamishak Bay in Lower Cook Inlet, 20 km from shore in 160 m of water. Spray icing also occurred on the nearby drill rig *Dan Prince*, however weather information is available only for the *Ocean Bounty* location. In this region wind speeds can vary dramatically over short distances because of funneling and channeling of winds through gaps in the nearby mountains so the conditions at the location of the *Dan Prince* might have been significantly different. The *Ocean Bounty* is 107-m long, 81-m wide, with the main deck 16 m above the ocean surface. Anemometer height was 276 ft (84 m) asl.

From September 24, 1979, to April 26, 1980, it experienced 21 days of sea spray icing on the superstructure in six icing storms lasting between 1 and 7 days each. During these events meteorological and oceanographic data as well as ice accumulation rates were recorded by OCEANROUTES meteorologist-observers every 2 hours from 6 am to 6 pm and at 10 pm and 2 am for a total of nine observations each day. Ice accumulations were recorded as light, moderate, heavy, very heavy, or extreme, corresponding to roughly 2, 3, 4, 6, or 10 in. of ice accumulated per day, respectively. The water temperature ranged from 4.4°C to 5.6°C.

Williams (1981) describes typical storms in the Cook Inlet area. Strong west-northwesterly orographic winds spilling through Kamishak Gap across lower Cook Inlet occur with a trough of low pressure oriented parallel to the mountain range over the Inlet. These conditions occur with rising pressures following an intense low, with cold air pooling over the Iliamna Basin. Strong northeasterlies are associated with high pressure over interi-
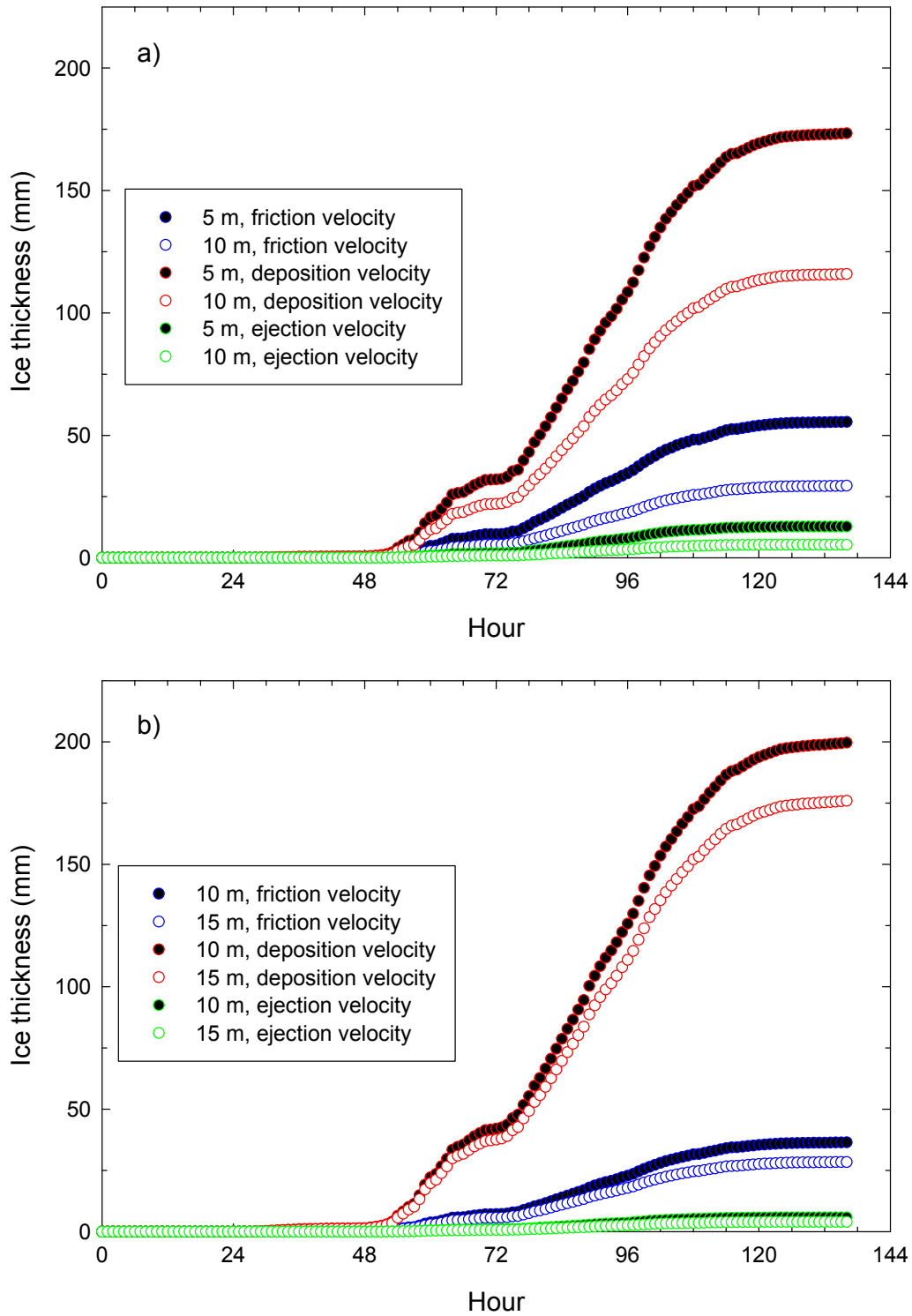
Figure 11. Modeled ice accretion on *Sedco 708*, (a) on a 30-cm-diameter cylinder at 5 and 10 m (like the diagonal trusses), (b) on a 2-cm-diameter cylinder (like the cylinder arrays) at 10 and 15 m.

or Alaska and a low southwest of the Inlet. Strong winds from the east-southeast are associated with low pressure systems moving northward into the Gulf of Alaska or Bering Sea. While the *Ocean Bounty* was on station, icing was primarily associated with west-northwesterly winds.

Wave height, wind speed, air temperature, relative humidity, and ice accumulation estimates are provided in tables grouped by wind direction in Nauman (1984). Concurrent weather, wave, and icing conditions can be recreated from these tables, assuming that the data are in the same order in all five tables. However, the chronological order has been lost, so these observations cannot be associated with particular storms. Air temperature data are plotted in Figure 12 in the top panel, with measured wind speed and the calculated 10-m wind in the middle panel, and measured and calculated significant wave height in the bottom panel. Lines are drawn through the data points that are grouped by wind direction only to make the plots easier to read. It was significantly colder and windier in these icing events than in the *Sedco 708* event. The significant discrepancy between the measured and calculated significant wave heights here is in contrast to the *Sedco 708* location. The wave heights are constrained by the short fetch, particularly for winds with a westerly component.

Modeled icing rates on 2-cm-diameter cylinders at 10 and 40 m asl for the three sea surface concentration distribution estimates are shown in Figure 13 along with the rough estimates of the daily rate of ice accumulation. Note that the icing rate at 40 m is not significantly smaller than the icing rate at 10 m, near the level of the main deck for any of three droplet velocity assumptions. The vertical scale for the top three panels in this figure is equivalent to the scales for the bottom panel: 1 in. of ice accumulation per day is essentially 1 mm per hour. The icing rate based on deposition velocity is too high by a factor of 10. On the other hand, the rate based on ejection velocity is near zero in many hours when significant icing was observed. The friction-velocity-based icing rate appears to best match the observations.

Ocean Bounty time series

Late in this study, MMS provided a file of the scanned *Ocean Bounty* handwritten daily Oceanographic and Meteorological Data Summary sheets. Some of the pages were too light to read, and on some generally readable pages some entries were illegible. Summary sheets for a few days

were missing. Within these constraints, we created an electronic file of the data for days with at least one recorded air temperature at 32°F or below.
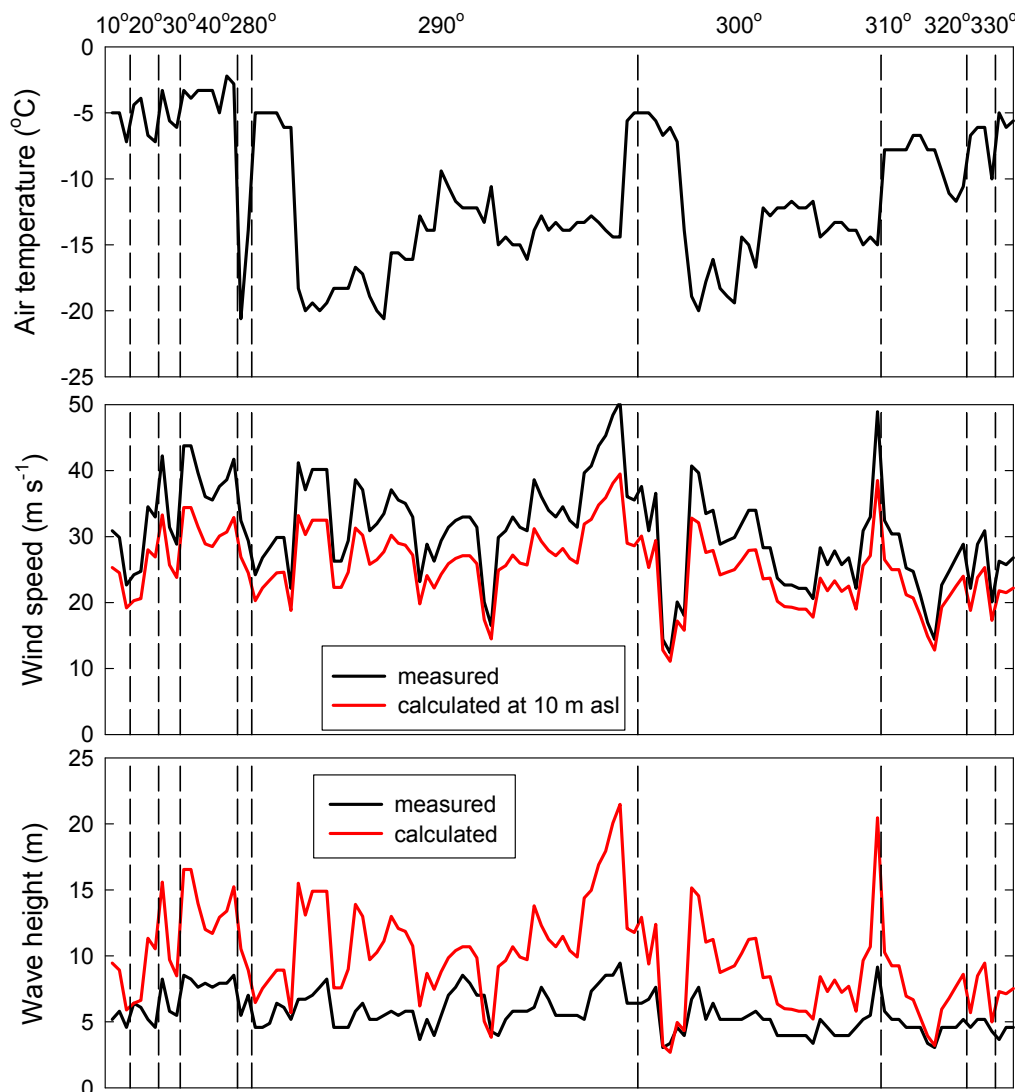
Figure 12. *Ocean Bounty* air temperature, wind speed (measured and corrected to 10 m asl), and measured and calculated significant wave height. Vertical lines group the values by wind direction.

Most weather and sea parameters were recorded every 2 hours from 0600 to 1800. In addition, maximum wave height, wind direction, wind and gust speed, air temperature, and barometric pressure were recorded at 0200 and 2200. Water temperature was measured at 1400 almost every day. When sea spray resulted in ice accreting on the *Ocean Bounty*, observers also visually estimated the severity of icing, designating it as light, moderate, heavy, very heavy, or extreme. The corresponding numerical

values of 2, 3, 4, 6, and 10, roughly interpreted as inches of ice per day, were recorded on the data sheets between 0600 and 1800. The relevant oceanographic, meteorological, and icing data from the handwritten summary sheets are provided in Appendix B. The 21 days with spray icing (Nauman 1984) are in red.
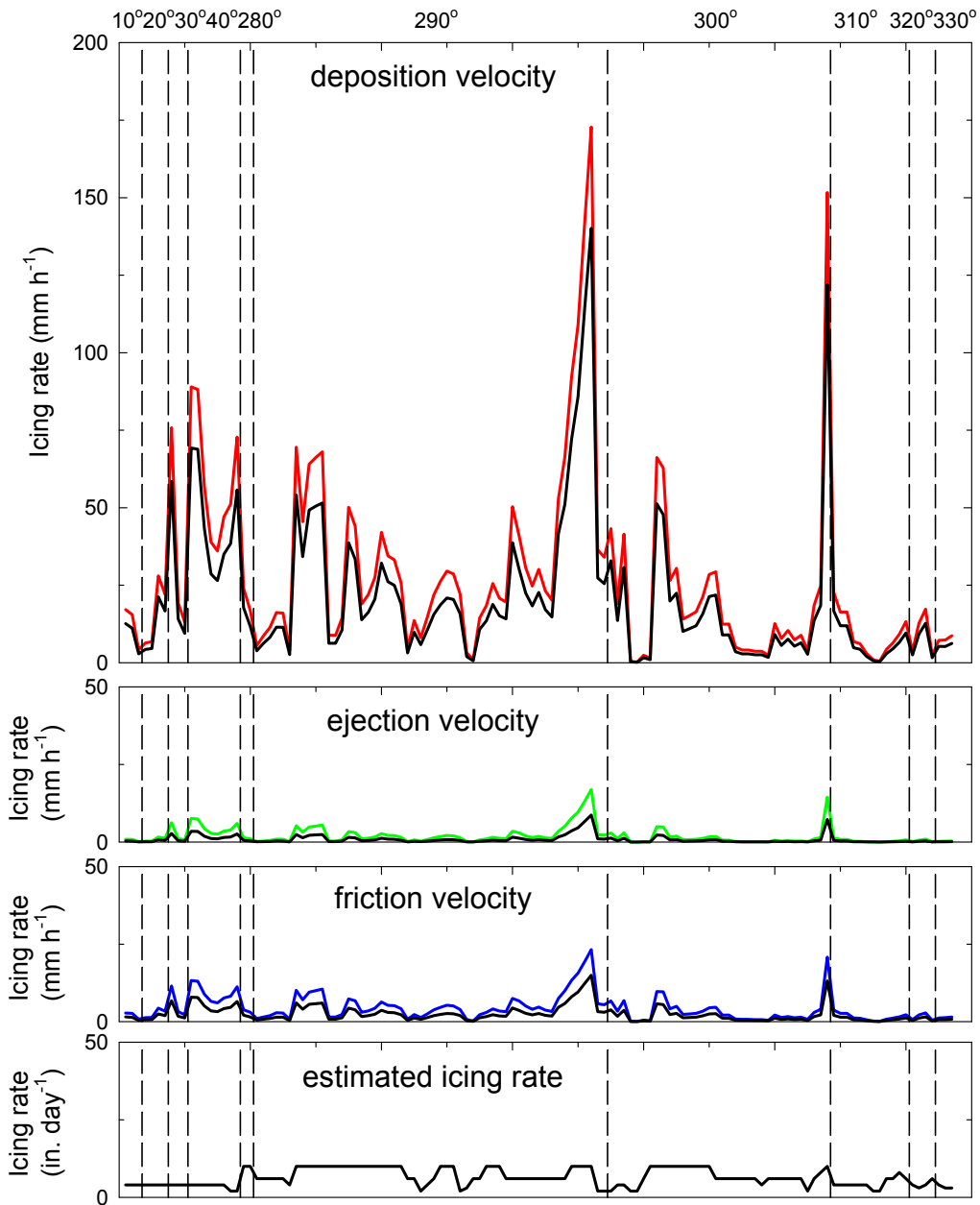
Figure 13. Icing rate on 2-cm-diameter cylinders at 10 (top line in each pair) and 40 m (lower line in each pair) on the *Ocean Bounty* for the three droplet velocity assumptions, compared to the estimated icing rate. Values are grouped by wind direction.

We again modeled spray icing as described in Section 3. We handled missing data (typically at 0200 and 2200) by filling in with data from the nearest hour. Results are shown in Figure 14. The measured wind speed corrected to 10 m asl is shown in the top panel along with the observed significant wave height in red. The second panel displays the air temperature (black) and water temperature (red). The observed icing severity is shown in the third panel, with the icing severity observation converted into the rough equivalent in inches per day, which is essentially the same as millimeters per hour. Modeled icing rates using the ejection, deposition, and friction velocity to calculate the liquid water content distribution from the flux are shown in the bottom three panels. As seen in the previous section, using the deposition velocity results in excessively high icing rates. Ejection and friction velocity results, on the other hand, are in the right range.

Some of the modeled spray icing events were not observed on the *Ocean Bounty*. The most significant was at the beginning of December in 1979. A possible explanation for the lack of accreted ice is the relatively warm ocean temperatures (6°C) and air temperatures (-7°C) in the days from 1979.94 to 1979.95. This result suggests that incorporating a heat balance calculation in the spray icing model would improve its performance.
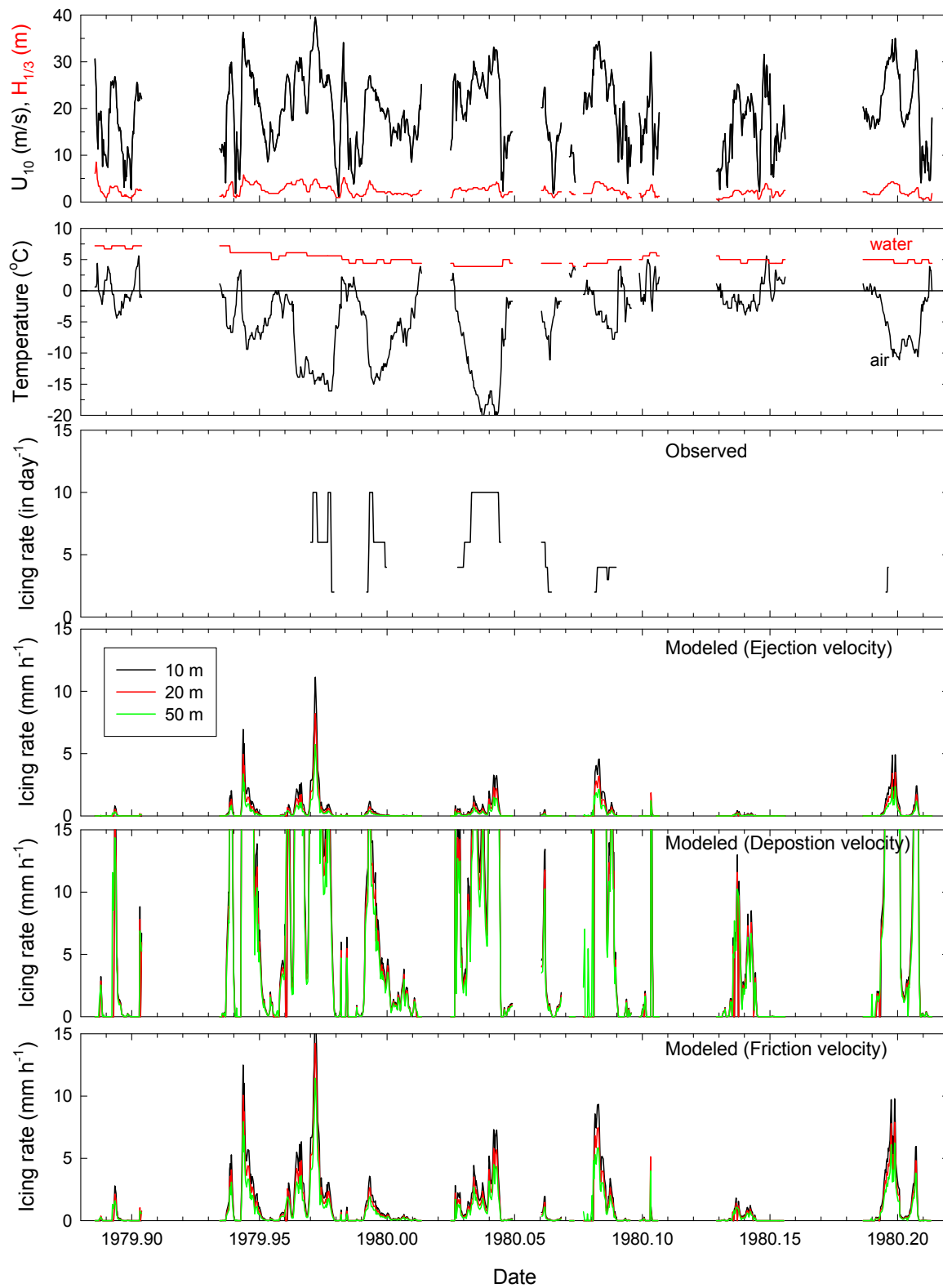
Figure 14. *Ocean Bounty* time series with modeled spray icing rates at 10, 25, and 50 m asl.

5   Discussion

Droplet concentration at the surface

A crucial required input to an ice accretion model for sea spray icing is the variation of the spray droplet concentration with height above the ocean surface. While we can specify the spray droplet flux at the ocean surface, determining the spray concentration proved to be surprisingly difficult. The problem boils down to answering the question "How fast are the droplets moving?"

Our first attempt—following the lead of others in the sea spray field—was to say that at equilibrium the upward flux of droplets from the surface must equal the downward flux; then, the spray droplet deposition velocity is the correct speed to use. However, this results in droplet concentration densities at the ocean surface that are an order of magnitude too high compared to measured values in the film droplet size range and most of the jet droplet range. And, in fact, the upward flux of droplets in these size ranges may be significantly different than the downward flux as the droplets evaporate from their radius at formation to a radius in equilibrium at the relative humidity of the air. As they evaporate, their settling velocity decreases, and they are carried more easily aloft by the turbulence in the air. A particular droplet may remain aloft, evaporating to a salt particle, or may fall back into the ocean miles away from where it was formed, with a smaller radius.

Our second attempt was to use the measured ejection velocity of jet droplets as they are formed by collapsing bubbles. This incorrectly treats film and spume droplets as jet droplets and assumes that the droplets retain that high (except for the very largest droplets) initial velocity over a significant distance rather than being slowed by drag. For droplets with a radius of up to about 15 μm, this assumption results in droplet concentration densities at the ocean surface that are an order of magnitude too low compared to measured values. However, ejection and deposition velocities are roughly the same for large droplets, so spume droplet concentration densities are equally well represented by either of these two velocity assumptions. It should be noted, however, that the calculated concentration distribution in this size range is smaller than measured values, implying that these droplets are moving more slowly than we expect.

Finally, we used the friction velocity to parameterize the vertical velocity of the droplets. This choice is intrinsically different from the other two approaches in that the droplet motion is associated with the wind and atmospheric stability rather than being a property of the droplet. This choice provided the best agreement between measured and calculated concentration distributions but, like the other two, resulted in smaller than measured values in the spume range.

The friction velocity assumption provided the best agreement with the limited information we had for two cases of spray icing on drill rigs. This choice, however, does not provide the observed shape of the ocean-level concentration distribution. Because friction velocity does not vary with droplet size, the concentration distribution has the same shape as the spray generation function dF/dr_{80}.

Whitecaps and significant wave height

Both the whitecap coverage and the significant wave height can be calculated from the wind speed at 10 m. The parameterization for the significant wave height (Equation 8) is based on buoy data from the North Atlantic. This formulation provided an excellent match to the *Sedco 708* observations, indicating that the very poor match to the *Ocean Bounty* observations is likely not because of some intrinsic difference between wind waves in Alaskan waters and in the Atlantic. The *Ocean Bounty* significant wave height discrepancy probably results from the limited fetch at the drill rig's location in Lower Cook Inlet.

The relatively small significant wave heights in Cook Inlet might also imply that the calculated whitecap coverage from Equation 9 is higher than actually occurred. The maximum *Ocean Bounty* wind speeds resulted in calculated whitecap covers of nearly 100%. The relatively small wind waves might imply fewer breaking waves and therefore fewer bubbles and fewer film and jet droplets than is expected for those wind speeds in open ocean conditions. However, the shearing of spume droplets off wave crests by the wind should not be diminished. It would be useful to test the Piazzola et al. (2002) fetch-limited whitecap parameterization, not only with the *Ocean Bounty* data but also with whitecap observations in limited fetch conditions.

Wind and icing data

The available weather and icing data for sea spray icing on offshore structures was very limited. We still expect to get chronological *Ocean Bounty* weather data for the winter of 1979-1980 from MMS. It would be useful to process the data for that entire winter to determine how well our algorithms identify the significant spray icing events that Nauman (1984) listed.

Available wind and temperature data for Alaskan waters could be used to model spray ice accretion at those locations. In a study completed recently for MMS, Veltcamp and Wilcox (2007) compiled meteorological data from January 2001 through September 2006 from five MMS stations along the coast of the Beaufort Sea. The parameters measured included wind speed and direction, air temperature, humidity, and barometric pressure. Three of the stations are on islands, one is on a point of land surrounded by water on three sides, and one is 2 km inland from the Beaufort Sea. All except one of those stations is still operating under the auspices of the University of Alaska. Veltcamp and Wilcox also compiled wind data from 29 additional stations in the area, some of which were in operation for only a few months. Some of these hourly data extend as far back as 1984. The purpose of the study was to compile weather data to use in MMS's Oil Spill Risk Analysis, Coastal Zone Oil Spill, and oil weathering and near-shore circulation models. Those data could also be used with the National Snow and Ice Data Center maps of sea ice extent (http://nsidc.org/data/seaice_index/archives/index.html) and this sea spray icing model to determine the severity of spray icing on offshore structures in this region. The sea ice maps would be used to screen the high wind/cold weather events to extract only those that occurred with open water. It would be interesting to examine the history of modeled spray ice thicknesses to identify any changes associated with global warming.

References

Andreas, E. L 1989. *Thermal and size evolution of sea spray droplets*. CRREL Report 89-11. Hanover, NH: U.S. Army Cold Regions Research and Engineering Laboratory.

Andreas, E. L 1998. The atmospheric boundary layer over polar marine surfaces. In *Physics of ice-covered seas*, vol. 2, ed. M. Leppäranta, 715–773. Helsinki, Finland: Helsinki University Press.

Andreas, E. L 2002. A review of the sea spray generation function for the open ocean. In *Atmosphere-ocean interactions*, vol. 1, ed. W. Perrie, 1–46. Boston, MA: WIT Press.

Andreas, E. L, P. O. G. Persson, and J. E. Hare. 2008. A bulk turbulent air-sea flux algorithm for high-wind, spray conditions. *J. Phys. Oceanogr*. 38:1581–1596.

Andreas, E. L, and S. Wang. 2007. Predicting significant wave height off the northeast coast of the United States. *Ocean Eng*. 34:1328–1335.

Blanchard, D. C. 1963. The electrification of the atmosphere by particles from bubbles in the sea. In *Progress in oceanography*, vol. 1, ed. M. Sears, 71–202. New York: MacMillan Publishing.

Burk, S. D. 1984. The generation, turbulent transfer and deposition of the sea-salt aerosol. *J. Atmos. Sci*. 41:3040–3051.

de Leeuw, G. 1986a. Vertical profiles of giant particles close above the sea surface. *Tellus* 38B:51–61.

de Leeuw, G. 1986b. Size distributions of giant aerosol particles close above sea level. *J. Aerosol Sci*. 17:293–296.

de Leeuw, G. 1987. Near-surface particle size distribution profiles over the North Sea. *J. Geophys. Res*. 92:14,631–14,635.

de Leeuw, G., C. W. Fairall, E. L Andreas, M. D. Anguelova, E. R. Lewis, C. O'Dowd, M. Schultz, and S. E. Schwartz. (In preparation). Primary production of sea spray aerosol. *Quart. J. Roy. Meteor. Soc*.

Edson, J. B., and C. W. Fairall. 1994. Spray droplet modeling. 1. Lagrangian model simulation of the turbulent transport of evaporating droplets. *J. Geophys. Res*. 99(C12):22,295–25,311.

Fairall, C. W., J. D. Kepert, and G. J. Holland. 1994. The effect of sea spray on surface energy transports over the ocean. *Global Atmos. Ocean System* 2:121–142.

Fairall, C. W., and S. E. Larsen. 1984. Dry deposition, surface production and dynamics of aerosols in the marine boundary layer. *Atmos. Environ*. 18:69–77.

Finstad, K. F., E. P. Lozowski, and E. M Gates. 1988a. A computational investigation of water droplet trajectories. *J. Atmos. Oceanic Technol*. 5:160–170.

Finstad, K. F., E. P. Lozowski, and L. Makkonen. 1988b. On the median volume diameter approximation for droplet collision efficiency. *J. Atmos. Sci.* 45(24):4008–4012.

Gong, S. L., L. A. Barrie, and J.-P. Blanchet. 1997. Modeling sea-salt aerosols in the atmosphere. 1. Model development. *J. Geophys. Res.* 102(D3):3805–3818.

Hoppel, W. A., P. F. Caffrey, and G. M. Frick. 2005. Particle deposition on water: surface source versus upwind source. *J. Geophys. Res.* 110:D10206.

Hoppel, W. A., G. M. Frick, and J. W. Fitzgerald. 2002. Surface source function for sea-salt aerosol and aerosol dry deposition to the ocean surface. *J. Geophys. Res.* 107(D19):4382–4399.

Jones, K. F. 1996. *Ice accretion in freezing rain*. CRREL Report 96-02. Hanover, NH: Cold Regions Research and Engineering Laboratory. [Available online at http://www.crrel.usace.army.mil/techpub/CRREL_Reports/reports/CR96_02.pdf].

Jones, K. F. 1998. A simple model for freezing rain ice loads. *Atmospheric Research* 46:87–97.

Langmuir, I., and K. Blodgett. 1946. Mathematical investigation of water droplet trajectories. In *Collected works of Irving Langmuir*, 1960, 335–393. Elmsford, NY: Pergamon Press.

Minsk, L. D. 1984a. *Ice observation program on the semi-submersible drilling vessel SEDCO 708*. CRREL Special Report 84-2. Hanover, NH: Cold Regions Research and Engineering Laboratory.

Minsk, L. D. 1984b. *Assessment of ice accretion on offshore structures*. CRREL Special Report 84-4. Hanover, NH: Cold Regions Research and Engineering Laboratory.

Minsk, L. D. 1985. Measurement of icing on offshore structures. In *Proceedings of the International Workshop on Offshore Winds and Icing*, ed. T. A. Agnew and V. R. Swail, 287–292. Downsview, Ontario, Canada: Atmospheric Environment Service.

Monahan, E. C. 1968. Sea spray as a function of low elevation wind speed. *J. Geophys. Res.* 73:1127–1137.

Monahan, E. C. 1986. The ocean as a source for atmospheric particles. In *The role of air-sea exchange in geochemical cycling*, ed. P. Buat-Ménard, 129–163. Dordrecht, The Netherlands: D. Reidel Publishing.

Monahan, E. C., F. W. Fairall, K. L. Davidson, and P. J. Boyle. 1983. Observed inter-relations between 10 m winds, ocean whitecaps and marine aerosols. *Quart. J. R. Met. Soc.* 109:379–392.

Monahan, E. C., and I. O. Muircheartaigh. 1980. Optimal power-law description of oceanic whitecap coverage dependence on wind speed. *J. Phys. Oceanogr.* 10:2094–2099.

Monahan, E. C., D. E. Spiel, and K. L. Davidson. 1986. A model of marine aerosol generation via whitecaps and wave disruption. In *Oceanic whitecaps and their role in air-sea exchange*, ed. E. C. Monahan and G. Mac Niocaill, 167–174. Dordrecht, The Netherlands: D. Reidel Publishing.

Nauman, J. W. 1984. Superstructure icing on the semi-submersible Ocean Bounty in Lower Cook Inlet, Alaska. In *Proceedings of the 2nd International Workshop on Atmospheric Icing of Structures, June, Trondheim, Norway*, 71–79.

Nauman, J. W., and R. Tyagi. 1985. Sea spray icing and freezing conditions on offshore oil rigs—Alaska experience and regulatory implications. In *Proceedings International Workshop on Offshore Winds and Icing*, *7–11 October, Halifax, Nova Scotia*, 313–328.

Overland, J. E. 1990. Prediction of vessel icing for near-freezing sea temperatures. *Wea. Forecasting* 5:62–77.

Overland, J. E., C. H. Pease, R. W. Preisendorfer, and A. L. Comiskey. 1986. Prediction of vessel icing. *J. Climate Appl. Meteor.* 25:1793–1806.

Pattison, M. J., and S. E. Belcher. 1999. Production rates of sea-spray droplets. *J. Geophys. Res.* 104(C8):18,397–18,407.

Piazzola, J., P. Forget, and S. Despiau. 2002. A sea spray generation function for fetch-limited conditions. *Annales Geophysicae* 20:121–131.

Pruppacher, H. R., and J. D. Klett. 1978. *Microphysics of clouds and precipitation*. Dordrecht, The Netherlands: D. Reidel Publishing.

Ryerson, C. C., and A. J. Gow. 2000. *Ship superstructure icing: crystalline and physical properties*. ERDC/CRREL Technical Report TR-00-11. Hanover, NH: Cold Regions Research and Engineering Laboratory.

Slinn, S. A., and W. G. N. Slinn. 1980. Predictions for particle deposition on natural waters. *Atmos. Environ.* 14:1013–1016.

Slinn, W. G. N., L. Hasse, B. B. Hicks, A. W. Hogan, D. Lal, P. S. Liss, K. O. Munnich, G. A. Sehmel, and O. Vittori. 1978. Some aspects of the transfer of atmospheric trace constituents past the air-sea interface. *Atmos. Environ.* 12:2055–2087.

Stramska, M. 1987. Vertical profiles of sea salt aerosol in the atmospheric surface layer: a numerical model. *Acta Geophys. Polonica* 35:87–100.

Veltkamp, B., and J. R. Wilcox. 2007. *Study final report for the nearshore Beaufort Sea meteorological monitoring and data synthesis project*. Prepared for the U.S. Dept of the Interior, Minerals Management Service, Alaska OCS Region.

Williams, J. A. 1981. Charting heavy Alaskan weather. *Offshore* June 5, 1981:49–54.

Wu, J. 1988. Variations of whitecap coverage with wind stress and water temperature. *J. Phys. Oceanogr.* 18:1448–1452.

Appendix A

Diffusive velocity V_a

From de Leeuw et al. (in preparation),

$$V_a = \frac{C_{Dz}^{1/2}}{k} 10^{-3/\mathrm{St}} u_* + \frac{k u_*}{R_p}.$$ (A-1)

C_{Dz} is the drag coefficient at height z. St is the Stokes number

$$\mathrm{St} = \frac{V_g u_*^2}{\nu g},$$ (A-2)

where g is the acceleration of gravity. R_p is a molecular diffusion term

$$R_p = \ln\left(\frac{2\Lambda \mathrm{Sc}^{1/2}}{\pi}\right) + \Lambda \mathrm{Sc}^{1/2},$$ (A-3)

where Sc is the droplet Schmidt number

$$\mathrm{Sc} = \frac{\nu}{D_d}.$$ (A-4)

D_d is the molecular diffusion of droplets (Pruppacher and Klett 1978, p. 361)

$$D_d = \frac{\kappa T (1 + \alpha Kn)}{6\pi\rho\nu r},$$ (A-5)

where $\kappa \, (=1.3806503 \times 10^{-23}\,\mathrm{J/K})$ is the Boltzmann constant, T is the absolute temperature (in Kelvin), ρ is the air density, and r is the droplet radius. Kn is the Knudsen number

$$\mathrm{Kn} = \frac{\lambda_a}{r},$$ (A-6)

where λ_a is the mean free path of air molecules. Also in Equation A-5 (Pruppacher and Klett 1978, p. 361),

$$\alpha = 1.257 + 0.400 \exp\left(\frac{-1.10}{\mathrm{Kn}}\right). \tag{A-7}$$

We calculate these parameters as well as u_* and several other micrometeorological quantities in the marine atmospheric surface layer from the bulk flux algorithm developed by Andreas et al. (2008) using the mean wind speed, air temperature and humidity, surface temperature and salinity, and barometric pressure.

Appendix B

Ocean Bounty time series

Date	Hour	Sig H ft	Max H ft	Dir N	Wind kt	Gust kt	Tair °F	Twater °F	Tdew °F	P mb	Icing
11/19/79	2		20	50	58	74	34			977.3	
	6	20	32	30	75	93	33		32	968.5	
	8	22	34	40	65	90	33		32	966.5	
	10	28	41	50	58	75	33		31	964.4	
	12	23	32	60	38	50	34		33	963.1	
	14	16	24	110	32	42	40	45	36	961.7	
	16	14	22	290	25	35	36		34	962.1	
	18	11	20	290	44	50	32		31	963.8	
	22		15	300	40	47	31			965.5	
11/20/79	2		14	300	45	50	30			967.2	
	6	7	13	300	32	38	28		27	972.9	
	8	6	11	300	16	24	29		27	977.0	
	10	6	11	210	30	48	32		30	980.7	
	12	5	10	220	24	34	31		30	983.4	
	14	4	7	170	22	30	34	44	22	984.8	
	16	4	7	180	22	30	35		30	986.1	
	18	3	6	180	22	28	35		24	987.8	
	22		5	180	17	22	35			989.2	
11/21/79	2		3	30	16	23	39			985.8	
	6	6	11	40	47	61	38		27	978.7	
	8	9	17	30	46	65	37		27	975.3	
	10	11	20	350	45	60	37		25	972.2	
	12	11	20	300	62	71	34		25	968.5	
	14	10	18	300	60	69	34		28	969.5	
	16	10	18	290	60	70	32	45	28	966.5	
	18	10	19	290	62	69	31		30	965.8	
	22			300	58	66	31			967.8	
11/22/79	2			300	64	72	27			969.5	
	6	11	19	290	60	67	25		19	972.9	
	8	11	19	280	47	55	24		18	976.6	
	10	11	19	290	46	54	25		17	978.7	
	12	10	18	290	38	46	25		19	981.0	
	14	8	15	310	37	45	25		21	983.1	
	16	7	13	310	34	44	26	45	23	983.7	
	18	7	13	310	36	45	26		23	985.4	
	22			310	34	41	25			989.2	
11/23/79	2			300	24	31	29			993.2	
	6	4	7	290	22	29	27		25	997.0	

Date	Hour	Sig H ft	Max H ft	Dir N	Wind kt	Gust kt	Tair °F	Twater °F	Tdew °F	P mb	Icing
	8	4	7	270	13	19	28		26	1000.7	
	10	4	7	240	6		29		28	1000.3	
	12	5	8	210	19	26	31		17	1005.8	
	14	4	7	200	9	12	31	44	20	1006.8	
	16	5	8	280	12	17	30		23	1008.1	
	18	4	7	290	11	17	31		26	1009.8	
	22			300	26	32	30			1012.5	
11/24/79	2			310	21	27	30			1012.9	
	6	3	5	290	19	24	29		22	1012.9	
	8	3	4	260	6	14	30		22	1012.5	
	10	2	3	260	5	11	31		25	1012.2	
	12	3	4	190	17	25	31		25	1010.8	
	14	4	6	190	29	37	32		20	1009.1	
	16	4	7	190	34	45	32	45	16	1008.1	
	18	5	9	170	33	42	32		19	1006.1	
	22			160	50	59	34			1003.7	
11/25/79	2			140	54	61	38			999.7	
	6	9	17	130	62	72	39		28	995.6	
	8	9	17	130	61	72	39		34	995.3	
	10	8	15	130	52	62	41		35	994.2	
	12	8	16	130	54	66	42		36	992.9	
	14	8	15	130	52	64	39	45	35	991.2	
	16	9	20	280	55	62	30		29	992.2	
	18	8	16	270	54	62	31		24	993.2	
	22				52	68	30			997.0	
12/07/79	2			30	25	40	34			1011.2	
	6	4	7	20	24	34	33			1009.8	
	8	4	7	340	23	34	32			1010.5	
	10	5	8	320	27	3	31			1010.2	
	12	5	8	310	26	38	30			1009.8	
	14	4	7	300	25	32	31	45	20	1008.8	
	16	3	5	310	21	28	30		22	1008.5	
	18	4	7	300	28	36	30		22	1008.5	
	22		4	300	8	16	30			1007.8	
12/08/79	2		8	290	48	54	22				
	6	8	15	290	53	65	21		18	1009.1	
	8	9	17	290	55	67	21		16	1010.2	
	10	11	20	280	54	71	21		16	1011.9	
	12	12	23	290	69	84	21		16	1011.9	
	14	12	23	290	71	84	22	43	16	1014.2	
	16	13	25	290	66	81	20		16	1016.9	
	18	14	27	290	72	83	20		16	1018.6	
	22		25	290	58	71				1023.7	
12/09/79	2		13	290	46	54	24			1024.4	

Date	Hour	Sig H ft	Max H ft	Dir N	Wind kt	Gust kt	Tair °F	Twater °F	Tdew °F	P mb	Icing
	6	4	7	300	21	27	25		22	1023.7	
	8	3	4	140	3	9	27		23	1022.7	
	10	3	5	190	13	19	28		27	1021.0	
	12	5	9	160	34	41	31		30	1018.3	
	14	5	7	160	24	33	33	43	30	1015.9	
	16	4	7	180	25	31	36		31	1013.2	
	18	4	6	250	15	21	35		30	1012.5	
	22	3		250	10	15	37			1011.2	
12/10/79	2			250	28	44	38			1010.2	
	6	11	20	280	70	85	26		23	1015.2	
	8	13	25	290	85	104	24		20	1015.2	
	10	16	32	300	90	104	23		19	1015.9	
	12	19	36	290	81	97	23		19	1020.7	
	14	17	33	300	86	100	22		16	1023.4	
	16	17	33	300	77	92	22		16	1026.1	
	18	15	29	290	72	85	20		16	1026.8	
	22		29	290	69	84	15			1023.8	
12/11/79	2		25	290	73	85	15			1028.8	
	6	14	25	290	73	84	18		10	1029.1	
	8	13	25	290	70	82	18		10	1028.4	
	10	12	23	290	64	73	19		10	1028.4	
	12	12	23	290	67	77	19		10	1027.1	
	14	12	23	290	63	72	19		9	1027.4	
	16	12	23	290	66	78	20		10	1026.1	
	18	12	23	290	66	78	19		9	1024.7	
	22		23	290	63	81	18			1021.3	
12/12/79	2			20	48	65	18			1023.7	
	6	14	27	10	56	82	20		13	1025.4	
	8	15	29	10	56	79	21		14	1024.7	
	10	14	27	20	57	84	21		14	1026.1	
	12	13	24	20	49	72	22		19	1026.8	
	14	13	24	10	52	78	20	43	16	1028.4	
	16	13	24	20	47	71	20		16	1026.8	
	18	12	23	20	49	71	20		16	1027.1	
	22		23	20	45	67	18		16	1027.4	
12/13/79	2		14	20	40	55	20			1026.1	
	6	8	15	360	35	51	20		14	1026.1	
	8	8	15	360	32	47	22		17	1025.7	
	10	8	15	360	35	47	22		16	1026.1	
	12	8	15	360	32	47	24		15	1025.7	
	14	7	13	360	28	43	24	43	15	1025.4	
	16	7	13	350	29	40	23		17	1025.4	
	18	7	12	350	26	38	22		18	1025.1	
	22		10	340	18	26	22				

Date	Hour	Sig H ft	Max H ft	Dir N	Wind kt	Gust kt	Tair °F	Twater °F	Tdew °F	P mb	Icing
12/14/79	2		6	360	20	29	24			1027.1	
	6	6	11	10	29	43	24		17	1027.4	
	8	6	11	20	39	52	25		20	1028.1	
	10	6	11	30	34	48	25		21	1029.1	
	12	6	11	30	34	45	29	41	22	1030.1	
	14	6	11	30	35	45	29		25	1030.8	
	16	6	11	30	31	44	30		24	1031.2	
	18	6	11	40	27	46	31		28	1033.2	
	22		10	40	24	58				1031.8	
12/15/79	2		10	40	26	37	32			1031.2	
	6	6	11	40	30	42	31		28	1029.5	
	8	6	11	40	31	41	31		28	1028.4	
	10	6	11	40	33	44	32		30	1027.1	
	12	6	11	40	33	45	32		28	1025.4	
	14	7	12	40	32	48	31	42	29	1023.4	
	16	7	13	40	42	57	30		29	1021.0	
	18	8	15	40	43	56	29		27	1018.6	
	22		16	20	46	58	28		26	1013.2	
12/16/79	2		18	20	46	58	24			1005.1	
	6	9	17	30	45	60	27		24	999.7	
	8	10	19	40	46	67	29		24	997.0	
	10	11	21	30	52	68	30		26	993.9	
	12	11	21	20	59	75	31		27	990.9	
	14	12	22	20	62	80	31	43	25	988.2	
	16	13	25	20	65	79	31		27	986.1	
	18	13	25	20	66	80	30		27	984.4	
	22		26	20	64	81	29			981.0	
12/17/79	2		21	20	60	79	28			978.3	
	6	13	25	10	48	69	28		25	976.0	
	8	14	27	360	42	60	28		24	975.3	
	10	12	23	360	40	56	29		25	974.3	
	12	12	23	350	42	61	26			973.2	
	14	12	23	350	40	54	28			972.6	
	16	12	23	300	54	65	20			970.9	
	18	12	23	300	62	72	17			970.5	
	22		25	300	69	78	12			970.2	
12/18/79	2		256	300	72	82	8			970.9	
	6	15	27	300	70	83	7			972.6	
	8	15	27	290	66	80	7			973.9	
	10	15	28	290	69	82	7			975.3	
	12	15	28	290	74	93	7			974.9	
	14	16	30	290	73	92	8			977.3	
	16	16	30	290	68	83	10			978.3	
	18	16	30	290	74	86	9			978.7	

Date	Hour	Sig H ft	Max H ft	Dir N	Wind kt	Gust kt	Tair °F	Twater °F	Tdew °F	P mb	Icing
	22		30	290	61	73	7			979.0	
12/19/79	2		20	270	63	72	7			979.3	
	6	12	23	300	53	62	9			979.3	
	8	12	23	300	51	59	12			979.6	
	10	11	20	300	44	51	13			980.0	
	12	8	14	300	43	51	13			980.4	
	14	7	12	300	43	52	12	42		980.4	
	16	7	12	290	44	57	12			980.7	
	18	7	13	290	53	67	11			980.7	
	22			300	65	79	8			979.3	
12/20/79	2			300							
	6	12	23	310	78	88			8		
	8	12	24	290	79	95			9		6
	10	14	26	290	81	100			8		6
	12	15	28	290	88	110			7		10
	14	15	28	290	90	109			6		10
	16	16	30	300	95	111			5		10
	18	16	31	290	98	114			6		10
	22			290	92	109					10
12/21/79	2			300	81	96					
	6	13	25	290	78	85	7				6
	8	12	22	290	76	81	6				6
	10	10	18	290	60	77	7				6
	12	10	18	290	63	75	6				6
	14	10	18	290	67	78	7	42			6
	16	10	18	290	63	75	7				6
	18	10	17	290	61	72	8				6
	22			300	57	64	8				
12/22/79	2			300	57	70					
	6	10	17	300	60	71	5				6
	8	9	17	290	58	67	5				6
	10	10	18	300	64	73	6				6
	12	10	19	290	60	70	6				6
	14	11	19	290	64	75	5	42			10
	16	11	19	290	64	73	3				10
	18	11	20	290	62	75	3				10
	22			300	57	66	3			1004.9	
12/23/79	2			300	51	58	3			1005.4	
	6	8	15	300	43	49	7			1004.1	2
	8	8	14	290	39	47	8			1003.1	2
	10	7	13	290	32	39	13			1003.1	2
	12	6	11	300	25	32	16			1001.0	
	14	5	9	360	16	25	19	42		999.0	
	16	4	7	360	15	23	22			998.6	

Date	Hour	Sig H ft	Max H ft	Dir N	Wind kt	Gust kt	Tair °F	Twater °F	Tdew °F	P mb	Icing
	18	3	5	20	15	26	22			997.0	
	22			40	8		21			995.3	
12/24/79	2			140	1		22			992.2	
	6	3	5	40	25		28			985.8	
	8	5	9	50	32	44	28			982.4	
	10	7	13	50	51	66	27			977.3	
	12	12	22	120	52	57	36			971.9	
	14	13	25	110	64	81	36	41		966.8	
	16	14	27	100	74	96	35			961.4	
	18	17	35	100	85	113	35			958.0	
	22			40	51	75	34			954.3	
12/25/79	2			30	62	85	34			950.9	
	6	13	24	30	50	71	29			949.9	
	8	10	19	350	43	58	30			951.9	
	10	9	17	360	27	43	31			954.9	
	12	8	15	50	15	22	34			957.3	
	14	7	13	100	17	24	33	40		958.0	
	16	7	13	190	28	36	34			959.0	
	18	6	11	180	31	36	34			961.4	
	22			210	14	18	33			965.1	
12/26/79	2			160	12	17	33			964.5	
	6	3	5	160	8	13	36			964.9	
	8	3	5	320	9	15	34			970.9	
	10	4	7	320	18	23	33			972.9	
	12	5	8	300	27	32	32			973.6	
	14	5	9	290	31	36	32	41		975.3	
	16	6	10	290	34	38	30			977.7	
	18	5	9	290	26	30	30			979.0	
	22			300	24	30	29			983.4	
12/27/79	2			300	16	23	29			986.1	
	6	4	6	300	20	26	26			987.1	
	8	4	7	310	17	22	25			988.5	
	10	4	7	320	20	25	25			989.8	
	12	4	7	310	26	32	26			990.2	
	14	4	7	320	28	34	26	40		990.9	
	16	5	9	310	35	40	26			990.9	
	18	5	9	310	43	49	25			990.5	
	22				57	64	25			990.2	
12/28/79	2			300	57	66	23			994.9	
	6	9	18	290	57	67	15			997.6	2
	8	12	23	290	61	72	13			999.7	4
	10	13	25	290	63	75	11			1002.0	6
	12	15	28	290	64	74	10			1004.1	10
	14	14	26	290	64	74	10	40		1006.1	10

Date	Hour	Sig H ft	Max H ft	Dir N	Wind kt	Gust kt	Tair °F	Twater °F	Tdew °F	P mb	Icing
	16	12	23	290	61	71	10			1009.5	10
	18	12	23	280	57	72	7			1011.5	10
	22			290	57	68	6			1016.9	
12/29/79	2			300	55	64	5				
	6	9	17	300	55	65	6				6
	8	9	17	290	56	64	7				6
	10	8	15	300	50	59	7				6
	12	7	13	300	54	62	8				6
	14	7	13	300	50	61	8	41			6
	16	7	13	300	52	60	7				6
	18	7	13	290	51	59	7			1025.7	6
	22			300	48	56	6			1025.4	
12/30/79	2			300	44	49	8			1025.1	
	6	7	13	300	46	52	10			1023.7	6
	8	7	13	300	44	50	10			1022.4	6
	10	7	12	290	45	52	9			1021.7	6
	12	7	13	290	44	51	11			1020.7	6
	14	7	13	300	43	49	10	40		1019.3	6
	16	7	13	300	43	49	10			1019.0	6
	18	6	11	300	40	47	11			1019.0	4
	22			300	42	51	10			1018.0	
12/31/79	2			300	46	65	12			1017.6	
	6	7	13	310	44	52	13			1016.6	
	8	7	13	310	39	47	14			1016.9	
	10	7	13	320	38	47	15			1017.3	
	12	7	12	320	34	46	15			1017.3	
	14	6	11	360	26	31	19	41		1019.3	
	16	6	11	360	30	30	19			1017.3	
	18	5	9	360	32	38	18			1017.3	
	22			360	36	54	19			1018.3	
01/01/80	2			360	33	48	20			1018.0	
	6	6	11	10	34	44	20			1016.9	
	8	6	11	360	33	44	20			1016.0	
	10	5	10	360	31	43	22			1016.6	
	12	6	11	350	30	40	23			1015.1	
	14	6	11	360	38	46	22	41		1015.6	
	16	6	12	350	38	49	23			1015.6	
	18	6	11	320	36	46	22			1015.6	
	22			330	29	37	24			1015.9	
01/02/80	2			310	40	46	21			1014.9	
	6	5	8	310	42	48	19			1014.6	
	8	5	9	310	43	50	17			1014.6	
	10	6	11	300	45	55	19			1015.6	
	12	6	11	310	37	44	21			1015.6	

Date	Hour	Sig H ft	Max H ft	Dir N	Wind kt	Gust kt	Tair °F	Twater °F	Tdew °F	P mb	Icing
	14	6	11	310	33	38	21	41		1015.2	
	16	6	11	300	39	46	18			1016.6	
	18	6	11	300	40	45	16			1017.3	
	22			300	40	44	20			1019.0	
01/03/80	2			320	32	42	21			1021.7	
	6	5	9	310	31	36	21		16	1023.7	
	8	5	8	320	27	33	21		17	1024.7	
	10	4	6	350	20	25	25		17	1025.7	
	12	4	6	360	18	26	27		13	1026.8	
	14	4	6	202	21	31	27	40	18	1026.8	
	16	5	8	20	26	35	26		18	1027.4	
	18	5	9	30	29	42	25		16	1027.8	
	22			30	37	49	24			1028.4	
01/04/80	2			40	34	45	30			1028.1	
	6	5	9	50	30	43	31		25	1027.4	
	8	6	12	130	30		31		29	1026.8	
	10	6	11	110	33	38	33		31	1026.8	
	12	6	12	120	39	46	35		33	1025.1	
	14	7	13	120	46	55	37	40	35	1023.0	
	16	8	15	110	50	58	38		36	1021.3	
	18	8	15	100	48	59	39		38	1019.3	
	22			110	61	72	37			1014.2	
01/09/80	2			320	25	29	35			1033.5	
	6	3	5	300	30	36	35		22	1028.1	
	8	4	7	280	32	42	35		21	1024.7	
	10	6	11	290	52	64	37		23	1021.0	
	12	8	15	290	63	72	36		25	1018.3	
	14	8	15	290	64	77	34	39	22	1014.6	
	16	9	17	300	67	77	33		18	1012.5	
	18	9	17	290	66	78	27		16	1010.2	
	22			320	40	57	26			1014.6	
01/10/80	2			20	62	84	26			1013.5	
	6	9	17	10	60	90	23		11	1013.9	
	8	10	19	10	58	85	23		11	1015.2	4
	10	10	19	30	61	85	22		12	1016.3	4
	12	10	18	30	56	76	21		12	1016.6	4
	14	9	17	20	47	67	20		10	1015.9	4
	16	8	15	20	48	67	19		3	1014.9	4
	18	8	15	10	44	66	19		5	1013.5	4
	22			350	40	57	20			1011.2	4
01/11/80	2			310	43	52	17			1007.1	
	6	8	15	310	44	53	15		10	1002.4	
	8	7	14	320	39	49	14		11	1000.4	6
	10	8	15	310	48	57	12		10	998.0	6

Date	Hour	Sig H ft	Max H ft	Dir N	Wind kt	Gust kt	Tair °F	Twater °F	Tdew °F	P mb	Icing
	12	8	15	310	52	64	11		9	995.6	6
	14	9	17	310	56	68	13		11	992.2	6
	16	9	17	300	55	68	10		8	990.9	6
	18	9	17	300	55	69	9		7	987.5	6
	22			340	48	78	8			983.4	6
01/12/80	2			300	61	74	9			979.0	
	6	9	17	300	62	75	6		4	976.0	
	8	10	18	300	66	79	6		4	974.6	10
	10	10	19	290	72	89	4		2	973.9	10
	12	10	18	290	69	79	4		2	973.2	10
	14	10	19	290	68	81	3		1	973.6	10
	16	10	19	290	64	77	3		1	975.3	10
	18	10	19	300	66	70	2		-1	976.0	10
	22	10		290	61	72	2			976.0	10
01/13/80	2			300	58	70	1			976.0	
	6	9	17	300	56	67	-1		-3	974.3	
	8	9	17	300	57	66	-2		-4	974.3	10
	10	9	17	300	58	76	-3		-5	972.9	10
	12	9	17	290	60	74	-2		-4	972.2	10
	14	9	17	290	62	72	-4		-6	971.2	10
	16	10	18	290	65	76	-5		-7	970.5	10
	18	10	18	280	63	73	-5		-7	969.9	10
	22			290	57	68	-3			969.9	10
01/14/80	2			290	54	61			-4	970.9	
	6	8	15	290	51	60	-1		-3	969.9	
	8	8	15	290	51	60	-1		-2	969.9	10
	10	8	15	290	57	66	-1		-2	969.8	10
	12	9	17	300	65	73	0		-1	966.8	10
	14	10	19	290	75	85	2		-1	965.1	10
	16	11	21	290	72	83	1		0	966.8	10
	18	11	21	300	66	78	3		1	968.8	10
	22			290	64	74			4	970.2	10
01/15/80	2			300	68	77				972.2	
	6	12	22	290	80	94	-1		-3	974.9	
	8	12	22	300	79	90	-2		-3	977.7	10
	10	12	22	290	72	81	-4		-6	980.7	10
	12	12	23	290	78	91	-3		-5	981.0	10
	14	13	25	290	78	90	-4		-6	983.1	10
	16	14	27	290	78	98	-3		-6	984.4	10
	18	13	25	300	77	86	-4		-5	986.1	10
	22			300	65	75	-3			990.9	10
01/16/80	2			300	61	68	2			992.9	
	6	7	13	300	35	41	7		5	994.9	
	8	4	6	320	9	15	10		7	994.9	6

Date	Hour	Sig H ft	Max H ft	Dir N	Wind kt	Gust kt	Tair °F	Twater °F	Tdew °F	P mb	Icing
	10	4	6	170	11	17	21		18	993.9	
	12	3	5	270	13		21		19	993.6	
	14	3	5	290	4	10	18	41	17	993.6	
	16	4	7	310	16	24	16		15	994.2	
	18	5	8	320	31	36	18		17	994.2	
	22			320	25	30	18			995.6	
01/17/80	2			50	20	30	30			1037.6	
	6	5	9	40	30	40	29		25	1035.4	
	8	6	11	40	32	41	27		26	1037.3	
	10	7	14	40	29	39	28		27	1038.6	
	12	7	14	40	31	41	29		27	1038.6	
	14	7	13	40	32	43	28	40	27	1038.6	
	16	7	12	40	33	42	29		27	1037.6	
	18	7	13	40	34	44	29		27	1037.3	
	22			40	34	46	29			1036.9	
01/22/80	2			290	47	56	26				
	6	8	15	290	47	56	23		13	994.3	
	8	8	15	290	52	62	23		13	997.3	6
	10	9	16	290	55	66	23		12	1001.7	6
	12	11	21	290	58	68	23		14	1004.4	6
	14	11	20	290	58	67	21		14	1008.1	6
	16	9	17	300	43	50	21	40	17	1010.8	6
	18	8	15	310	39	48	19		15	1012.9	4
	22				35	42	18			1014.0	4
01/23/80	2			300	29	37	19			1035.1	
	6	6	11	310	33	38	12				
	8	6	10	310	28	37	12		9		2
	10	6	10	300	28	33	20		8	1029.8	2
	12	6	11	300	24	29	21		9		2
	14	5	9	300	21	26	22		6	1032.2	2
	16	4	6	320	7		23	40	9	1032.5	
	18	3	4	350	3	7	24		17	1033.5	
	22				5	11	25			1033.2	
01/24/80	2			50	20	30	30		25	1037.6	
	6	5	9	40	30	40	29		26	1035.9	
	8	6	11	40	32	41	27		27	1037.3	
	10	7	14	40	29	39	28		27	1038.6	
	12	7	14	40	31	41	29		27	1038.6	
	14	7	13	40	32	43	28	40	27	1038.6	
	16	7	12	40	33	42	29		27	1037.6	
	18	7	13	40	34	44	29		27	1037.3	
	22			40	39	46	29			1036.9	

Date	Hour	Sig H ft	Max H ft	Dir N	Wind kt	Gust kt	Tair °F	Twater °F	Tdew °F	P mb	Icing
01/26/80	2			130		31	37			1036.9	
	6	7	13	120	22	27	36		33	1036.6	
	8	6	12	110	28	33	36		35	1036.6	
	10	6	11	110	24	30	37		36	1037.6	
	12	5	9	110	24	30	38		35	1037.9	
	14	6	10	100	25	28	38	39	35	1037.3	
	16	5	9	140	25	30	39		33	1037.6	
	18	5	10	140	16		39		33	1037.6	
	22			140	10	20	38			1037.9	
01/27/80	2										
	6										
	8										
	10										
	12										
	14										
	16										
	18										
	22										
01/28/80	2			320	44	54				1026.8	
	6	6	11	320	56	65	31		24	1025.4	
	8	6	12	320	51	61	32		25	1025.1	
	10	6	11	320	56	66	32		29	1025.1	
	12	6	11	320	47	56	34		26	1024.0	
	14	6	10	320	47	55	35	40	26	1023.0	
	16	6	10	320	48	55	33		24	1022.0	
	18	6	11	310	53	59	31		25	1021.3	
	22			300	56	70	33			1015.9	
01/29/80	2			30	53	68	32			1015.2	
	6	6	11	20	48	56	32		24	1012.9	
	8	7	13	30	57	67	31		22	1010.8	
	10	9	17	30	69	87	31		22	1009.1	
	12	10	18	40	66	82	32		26	1009.1	
	14	13	25	30	82	97	31	40	26	1007.1	
	16	13	26	40	75	91	28		22	1006.4	
	18	14	23	40	81	94	27		20	1005.8	2
	22			40	83	94	25			1006.4	2
01/30/80	2			40	80	93	25				
	6	14	28	40	85	101	26		23	1002.0	4
	8	14	27	40	85	96	25		15	1001.4	4
	10	14	27	30	82	96	26		20	1000.0	4
	12	13	25	40	77	91	26		16	999.7	4
	14	13	26	40	70	81	26	40	17	998.0	4
	16	13	25	40	69	85	26		20	996.6	4
	18	13	26	40	73	86	23		18	995.9	4

Date	Hour	Sig H ft	Max H ft	Dir N	Wind kt	Gust kt	Tair °F	Twater °F	Tdew °F	P mb	Icing
	22										
01/31/80	2			30	74	91	23			989.5	
	6	11	21	20	67	77	24		14	986.5	
	8	11	20	20	64	70	25		16	985.1	4
	10	10	19	330	51	63	23		17	984.1	4
	12	8	15	330	50	59	21		17	982.4	4
	14	8	15	330	52	70	22	41	16	980.7	3
	16	9	17	320	56	69	21		17	979.0	3
	18	9	17	320	60	68	21		17	978.0	3
	22			320	59	69	21			976.0	4
02/01/80	2			310	68	76	21			973.9	
	6	10	19	310	63	71	18		17	973.9	
	8	9	17	310	59	69	18		15	974.9	4
	10	9	17	310	59	66	18		17	974.9	4
	12	8	15	310	49	56	18		17	974.9	4
	14	8	15	320	43	54	20	41	18	973.2	4
	16	8	15	310	48	53	20		18	973.6	4
	18	8	15	310	41	50	20		19	974.9	4
	22			320	35	41	20			976.0	4
02/02/80	2			300	19	29	38			971.2	
	6	8	15	130	48	58	38		33	968.5	
	8	7	13	120	38	46	39		32	968.2	
	10	6	11	110	32	41	39		32	967.5	
	12	5	9	300	21		33		30	966.5	
	14	5	9	40	20	31	36	41	34	964.8	
	16	5	9	20	22	31	34		33	964.4	
	18	7	13	310	50	55	34		33	964.4	
	22			300	51	57	33			966.1	
02/03/80	2			300	29	36	23			970.5	
	6	6	11	170	37	47	27		24	976.3	
	8	3	5	240	15	31	30		25	977.3	
	10	2	4	280	8	16	28		25	978.3	
	12	3	5	230	16	24	28		22	979.7	
	14	4	7	220	31	39	28	41	21	983.1	
	16	3	5	220	23	31	28		19	984.1	
	18	3	5	190	16	26	27		23	986.5	
	22			230	27	44	27			992.2	
02/04/80	2										
	6										
	8										
	10										
	12										
	14										
	16										

Date	Hour	Sig H ft	Max H ft	Dir N	Wind kt	Gust kt	Tair °F	Twater °F	Tdew °F	P mb	Icing
	18										
	22										
02/05/80	2			230	45	50	37			988.8	
	6	6	11	150	37	47	32		15	991.9	
	8	3	6	310	18	23	29		20	992.9	
	10	3	5	320	19	25	29		21	992.9	
	12	4	7	320	32	37	30		24	991.9	
	14	4	7	340	27	35	30	42	27	991.9	
	16	4	7	330	35	42	28		27	988.8	
	18	5	9	340	33	41	31		30	987.8	
	22			50	41	45	29			984.4	
02/06/80	2			50	34	38	38			980.0	
	6	8	15	120	55	63	41		40	976.3	
	8	8	15	110	50	57	41		40	976.6	
	10	8	15	130	49	58	40		39	976.6	
	12	8	15	140	50	63	40		38	977.0	
	14	9	17	140	55	64	39	43	38	977.3	
	16	11	21	230	77	88	33		29	980.0	
	18	12	22	220	79	90	30		27	983.7	
	22			280	50	65	26				
02/07/80	2			300	12	26	34			998.3	
	6	7	13	230	39	49	38		34	1004.4	
	8	3	9	220	34	41	39		31	1006.4	
	10	4	7	180	28	36	38		26	1009.1	
	12	4	7	190	25	37	32		26	1010.5	
	14	4	6	220	26	30	34	42	28	1011.9	
	16	3	5	190	20	25	34		27	1012.2	
	18	4	7	170	31	39	34		26	1012.5	
	22			160	45	32	36			1013.2	
02/16/80	2			320	14	17	34			1016.3	
	6	2	3	310	14	17	33		28	1016.6	
	8	1	2	330	15	18	32		30	1017.6	
	10	2	4	340	15	18	33		28	1013.9	
	12	2	4	350	10	13	32		26	1012.5	
	14	2	4	330	5		33	41	25	1011.2	
	16	2	4	310	15	18	34		26	1010.2	
	18	2	3	310	14	19	30		26	1009.5	
	22			330	16	25	32			1009.1	
02/17/80	2										
	6	3	4	330	29	34	28		20	1001.4	
	8	3	5	320	33	40	28		24	1000.4	
	10	3	4	330	21	27	28		25	1000.0	
	12	3	5	340	13	20	29		25	999.3	

Date	Hour	Sig H ft	Max H ft	Dir N	Wind kt	Gust kt	Tair °F	Twater °F	Tdew °F	P mb	Icing
	14	3	5	350	7		29	41	24	998.0	
	16	3	5	340	6		29		25	997.3	
	18	3	4	330	18	25	27		25	997.0	
	22										
02/18/80	2										
	6	4	8	320	38	45	27		23	988.5	
	8	4	7	350	20	26	30		25	988.8	
	10	5	9	350	36	47	30		20	988.5	
	12	7	13	30	52	61	30		18	986.8	
	14	7	14	30	50	65	31	41	23	986.1	
	16	8	15	30	57	68	31		27	986.1	
	18	8	15	20	52	62	29		21	985.8	
	22										
02/19/80	2			30	60	67	26			987.1	
	6	8	16	30	60	71	31		22	987.1	
	8	8	15	30	58	67	29		23	987.8	
	10	7	14	20	54	61	28		21	988.8	
	12	7	13	20	50	61	29		13	988.5	
	14	7	12	30	45	53	29	40	16	988.2	
	16	6	11	20	41	49	29		21	987.8	
	18	5	9	20	32	38	28		22	986.8	
	22			30	44	51	28			986.1	
02/20/80	2			40	41	48	26			984.8	
	6	6	11	40	45	53	25		24	983.4	
	8	7	13	30	43	49	26		24	984.1	
	10	7	13	30	49	59	26		24	984.4	
	12	8	15	40	50	60	27		25	983.7	
	14	8	15	40	53	61	27	41	25	982.4	
	16	8	15	40	52	60	27		27	981.4	
	18	7	14	40	51	60	28		28	981.4	
	22			40	45	57	26			982.1	
02/21/80	2			40	55	63				980.4	
	6	8	15	40	50	56	29		26	979.0	
	8	7	13	50	48	57	29		27	979.3	
	10	7	13	50	42	51	31		28	979.7	
	12	6	12	230	31	37	29		27	981.4	
	14	7	14	230	39	45	29		25	983.1	
	16	7	14	220	44	54	28	41	24	984.4	
	18	8	15	230	38	45	27		24	985.8	
	22			250	21		26			990.5	
02/22/80	2			260	9					993.6	
	6	2	4	30	4	9	28		23	993.2	
	8	3	4	150	13	19	31		22	994.2	
	10	4	7	100	35	42	34		27	994.2	

Date	Hour	Sig H ft	Max H ft	Dir N	Wind kt	Gust kt	Tair °F	Twater °F	Tdew °F	P mb	Icing
	12	5	9	50	36	46	34		29	993.2	
	14	7	15	90	36	44	36	41	33	991.9	
	16	8	15	40	54	68	34		31	988.5	
	18	9	18	60	62	73	34		32	985.4	
	22			110	78	108	34			978.7	
02/23/80	2			130	54	64	38			979.0	
	6	13	25	130	73	90	42		38	975.3	
	8	12	23	140	72	89	41		39	977.3	
	10	11	22	140	55	68	41		37	979.0	
	12	9	18	140	58	68	41		37	980.0	
	14	9	17	150	51	60	41	40	36	983.1	
	16	9	18	220	56	69	35		27	985.8	
	18	9	19	230	67	78	34		26	991.9	
	22	10		320	12	18	30			1001.0	
02/24/80	2			290	17	23	29			1006.8	
	6	3	4	350	11	16	30		26	1008.1	
	8	4	7	10	18	23	31		26	1008.1	
	10	5	8	40	29	35	32		31	1008.1	
	12	5	9	40	32	38	37		35	1007.5	
	14	7	13	110	33	38	38	40	31	1007.1	
	16	7	13	140	20	27	37		32	1007.1	
	18	7	13	50	39	43	35		29	1007.5	
	22			40	31	36	35			1008.1	
02/25/80	2			50	24	29	36			1010.5	
	6	4	6	40	27	30	35		28	1010.2	
	8	5	8	40	31	36	35		30	1009.2	
	10	5	9	30	34	39	35		28	10096.1	
	12	6	11	30	36	42	34		28	10096.1	
	14	6	11	20	38	43	34	41	29	1008.8	
	16	7	13	10	41	48	34		23	1007.8	
	18	8	15	360	49	57	34		22	1007.8	
	22			330	31	37	36			1006.1	
03/09/80	2			290	48	59	34			1007.8	
	6	7	13	290	45	50	32		23	1008.1	
	8	7	13	290	41	49	32		25	1008.8	
	10	7	13	300	44	52	32		25	1009.1	
	12	7	13	290	47	53	32		25	1009.1	
	14	7	13	300	45	52	33	41	25	1008.8	
	16	6	11	300	40	44	33		25	1009.1	
	18	6	11	300	44	49	32		26	1009.1	
	22			300	42	48	32			1009.1	
03/10/80	2			300	36	44	34			1009.5	
	6	5	9	300	38	44	33		24	1007.8	

Date	Hour	Sig H ft	Max H ft	Dir N	Wind kt	Gust kt	Tair ºF	Twater ºF	Tdew ºF	P mb	Icing
	8	5	9	300	42	47	31		23	1007.8	
	10	5	9	300	43	49	32		23	1008.1	
	12	5	9	310	43	47	32		24	1008.1	
	14	6	11	310	42	48	32	41	24	1007.8	
	16	5	9	310	40	45	33		21	1007.1	
	18	5	9	300	36	43	33		24	1006.4	
	22			310	38	46	31			1005.8	
03/11/80	2			310	41	48	30			1005.1	
	6	5	9	310	38	45	30		16	1005.1	
	8	5	9	310	41	43	30		17	1005.1	
	10	5	9	310	40	45	31		23	1005.4	
	12	6	11	310	44	46	31		23	1005.8	
	14	7	13	300	49	52	30	41	25	1005.8	
	16	7	13	310	54	55	29		26	1005.8	
	18	8	15	300	54	62	28		22	1005.8	
	22			300	55	63	26			1006.4	
03/12/80	2			300	58	66	25			1007.8	
	6	10	19	300	67	75	23		18	1009.5	
	8	11	21	300	70	79	22		17	1009.8	
	10	11	21	300	69	78	23		19	1010.5	2
	12	11	21	300	73	72	23		17		2
	14	12	22	300	73	72	23	41	18		2
	16	13	25	300	71	83	22		13	1010.2	4
	18	13	26	300	75	85	21		13	1010.2	4
	22			300	74	86	19			1010.9	
03/13/80	2			290	76	86	15			1009.5	
	6	14	27	300	85	88	15		11	1008.5	
	8	14	28	300	72	91	13		10	1008.8	
	10	14	28	300	77	87	15		13	1008.8	
	12	13	27	290	73	89	15	40	11	10058.5	
	14	13	25	290	78	91	14		10	1008.5	
	16	13	25	300	86	90	14		11	1008.5	
	18	13	25	300	81	91	14		10	1008.5	
	22			290	70	85	13			1008.5	
03/14/80	2			290	66	77	13			1007.5	
	6	12	22	300	62	75	12		10	1006.8	
	8	7	13	300	65	65	14		13	1005.4	
	10	7	13	300	45	68	14		12	1005.4	
	12	6	11	300	44	52	15	40	12	1003.4	
	14	6	11	310	41	52	17		13	1002.7	
	16	6	10	300	39	47	18		13	1001.4	
	18	6	10	300	39	45	18		13	1001.0	
	22			300	36	44	18			999.7	
03/15/80	2			300	38	45	16			999.0	

Date	Hour	Sig H ft	Max H ft	Dir N	Wind kt	Gust kt	Tair °F	Twater °F	Tdew °F	P mb	Icing
	6	5	9	310	42	47	16		13	997.6	
	8	5	8	300	43	47	16		10	997.6	
	10	5	9	300	40	50	18		15	998.0	
	12	4	7	300	41	47	18	41	15	98.0	
	14	5	9	300	44	48	19		15	998.3	
	16	5	9	310	43	51	19		17	997.3	
	18	6	11	310	45	54	19		17	997.3	
	22	7		310	50	57	18			997.3	
03/16/80	2			300	53	61	17			995.6	
	6	7	13	300	62	72	15		11	995.3	
	8	7	14	300	68	75	15		11	995.6	
	10	7	12	300	67	75	14		10	995.6	
	12	8	14	290	68	80	14	40	8	994.9	
	14	9	17	300	73	88	15		11	994.9	
	16	9	17	290	79	91	15		11	994.9	
	18	10	18	300	78	92	15		11	997.3	
	22			290	67	79	13			998.6	
03/17/80	2			300	48	54	17			998.3	
	6	3	5	320	13	26	20		15	996.6	
	8	3	5	100	8	12	25		19	995.3	
	10	3	5	100	10		27		25	994.9	
	12	2	3	50	26	35	28	41	22	992.9	
	14	2	3	50	26	30	26		26	992.6	
	16	2	3	30	19	32	29		27	992.9	
	18	2	3	30	22	31	28		27	993.9	
	22	4	3	70	13	21	30			996.6	
03/18/80	2			320	29	36	29		25	1002.4	
	6	3	5	330	25	28	29		25	1004.1	
	8	3	5	300	14	18	30		27	1006.1	
	10	3	5	300	18		30		27	1006.1	
	12	2	3	310	10	18	34	40	26	1006.4	
	14	0			0		39		28	1005.8	
	16	1	2	50	10		38		27	1005.4	
	18	1	2	50	18		38		27	1005.1	
	22	6		360	42	50	32			1006.4	

REPORT DOCUMENTATION PAGE

1. REPORT DATE *(DD-MM-YYYY)*	2. REPORT TYPE	3. DATES COVERED *(From - To)*
February 2009	Technical Report	

4. TITLE AND SUBTITLE

Technology Assessment and Research Program, Safety and Engineering Research
Sea Spray Icing of Drilling and Production Platforms

5a. CONTRACT NUMBER

5b. GRANT NUMBER

5c. PROGRAM ELEMENT NUMBER

6. AUTHOR(S)
Kathleen F. Jones and Edgar L Andreas

5d. PROJECT NUMBER

5e. TASK NUMBER

5f. WORK UNIT NUMBER

7. PERFORMING ORGANIZATION NAME(S) AND ADDRESS(ES)

Cold Regions Research and Engineering Laboratory
U.S. Army Engineer Research and Development Center
72 Lyme Road
Hanover, NH 03755-1290

8. PERFORMING ORGANIZATION REPORT NUMBER
ERDC/CRREL TR-09-3

9. SPONSORING / MONITORING AGENCY NAME(S) AND ADDRESS(ES)

10. SPONSOR/MONITOR'S ACRONYM(S)

11. SPONSOR/MONITOR'S REPORT NUMBER(S)

12. DISTRIBUTION / AVAILABILITY STATEMENT
Approved for public release; distribution is unlimited.

13. SUPPLEMENTARY NOTES

14. ABSTRACT
Because of the observed decrease in the ice cover in the Beaufort and Chukchi Seas, it is possible that spray icing of rigs used for oil exploration and drilling may be more frequent and possibly more severe in the coming years than it has been in the past. In this report we describe a model for sea spray icing on fixed offshore structures. The accretion of small sea spray droplets onto two-dimensional structural sections and components depends on the liquid water content of the spray cloud, as well as wind speed, droplet diameter, and the diameter of the object. The spray cloud's liquid water content is obtained from the flux of film, jet, and spume droplets from the ocean surface and the vertical velocity of the droplets. The spray droplet flux increases dramatically with increasing wind speed, as whitecaps cover more of the ocean surface and the wind shears droplets off the wave crests. The more massive larger droplets tend to fall out of the spray cloud; as a result, the liquid water content decreases with height. We present modeled icing rates for the semi-submersible drilling rigs *Ocean Bounty* in the winter of 1979-1980 and the *Sedco 708* in January 1983. These results are compared to available information on the icing rate or the ice accumulation.

15. SUBJECT TERMS
drill rigs; ice accretion; ice load; icing; liquid water content; ocean; offshore structures; sea spray

16. SECURITY CLASSIFICATION OF:

a. REPORT	b. ABSTRACT	c. THIS PAGE	17. LIMITATION OF ABSTRACT	18. NUMBER OF PAGES	19a. NAME OF RESPONSIBLE PERSON
U	U	U	U	63	19b. TELEPHONE NUMBER *(include area code)*